On the Nature of Potential Energy in Atmospheric Gravity Waves, or Why the Atmosphere Cannot Sustain a Tsunami

EMILE A. OKAL[1]

Abstract—Motivated by the generation of exceptionally large gravito-elastic waves during the Hunga Tonga–Hunga Ha'apai explosion of 15 January 2022, we examine theoretically the nature of the main air wave branch GR_0, whose undispersed celerity, ~ 313 m/s, suggests that it may represent a "tsunami" of the atmospheric column for an effective thickness $H_{eff} \approx 10$ km. However, we find that its potential energy is about 90% elastic across a wide frequency band, thus negating the widely held perception that it constitutes an oscillation between kinetic and gravitational energy. Based on the systematic study of the effect of finite compressibility on the dispersion and potential energy of a classic oceanic tsunami, we confirm that this feature of the branch GR_0 stems from the similarity between its celerity and the average speed of sound in the atmosphere. We then show that this similarity is not fortuitous, but rather expected for a perfect gas, which, we conclude, cannot sustain "tsunamis", i.e., oscillations between kinetic and gravitational energy.

Keywords: Ocean coupled air waves, tsunamis, 2022 Tonga explosion.

1. Introduction and Background: Are GR Modes the "Tsunamis" of the Atmosphere?

The explosion of the Hunga Tonga–Hunga Ha'apai (hereafter Tonga) volcano on 15 January 2022 generated gigantic atmospheric gravity waves recorded worldwide as barometric signals with amplitudes of a few hPa, including after circling the Earth several times at group velocities of ~ 313 m/s (e.g., Carvajal *et al.*, 2022; Gusman *et al.*, 2022). Because they are mostly concentrated in the atmospheric shell surrounding the Earth, such waves can be regarded as intrinsically *guided* by that structure,

and fall within the general family studied by Lamb (1910; hereafter L10), to the extent that they are generally called "Lamb waves". However, due to the finite elasticity of both the solid Earth and the oceanic column, they can couple to these media, including over essentially enclosed seas such as the Mediterranean, and thus were also recorded worldwide by seismic stations on land, marigraphs in ports, and ocean-bottom sensors on the high seas (Okal, 2022).

In historical times, natural predecessors to the Tonga air waves have followed the Krakatau explosion of 27 August 1883 (Ewing & Press, 1955), and at reduced amplitudes, the 1908 Tunguska meteorite explosion (Ben-Menahem, 1975), or even very large earthquakes, such as the 1964 Alaskan one (Okal & Talandier, 1991). In particular, Whipple (1930) noticed the agreement, in the range 310–320 m/s, between the air wave celerities observed during the Krakatau and Tunguska events, thus establishing their common physical nature. In addition, the large 1961 atmospheric nuclear tests over Novaya Zemlya, culminating with a 57-Mt explosion on 30 October 1961, also generated comparable waves (e.g., Donn & Ewing, 1962; Press & Harkrider, 1962; Wexler & Hass, 1962); even the first Soviet thermonuclear test, with a moderate yield of 3 Mt (22 November 1955), produced Lamb waves detected in Japan (Yamamoto, 1957). In this context, the 2022 Tonga explosion revived interest in the general properties of acoustic-gravity waves in the atmosphere.

From a theoretical standpoint, the study of atmospheric oscillations can be traced back to Laplace (1805, Chapter 5), with further landmark contributions by L10, Taylor (1937) and Pekeris (1937), who provided theoretical interpretations of the observed wave celerity, then taken as 318 m/s.

[1] Department of Earth and Planetary Sciences, Northwestern University, Evanston, IL 60208, USA. E-mail: emile@earth.northwestern.edu

However, most of these early studies focused on seeking a resonant response of the atmosphere to the forcing of the Earth by lunar and solar tides.[1] In addition, Laplace (1805) substantially simplified the problem by assuming for example that the particle displacement in the atmosphere was purely horizontal. While L10 later recognized such shortcomings, he kept the name "longitudinal waves", and himself retained debatable assumptions regarding the structure of the "Lamb wave", which will be discussed in Sect. 4.

After Ewing and Press (1955) first proposed the atmospheric nature of far-field marigraphic signals of the Krakatau explosion, Press and Harkrider (1962) used the context of atmospheric nuclear tests to give a comprehensive theoretical discussion of the various waves sustained by an atmospheric column, using the model of the Air Research and Development Command [ARDC] (Minzner *et al.,*1959; Wares *et al.,*1960), terminated by a free surface at an altitude of 220 km (their Figure 8, p. 3898, reproduced as Figure 2 of Harkrider & Press, 1967).

We recall these concepts in some detail since they provide the general framework of the waves observed during the Tonga explosion. As detailed, e.g., by Harkrider (1964) and in very simple terms, atmospheric air waves fall into two categories: *S* and *GR* modes. In the former, the restoring force upon mechanical deformation is purely elastic, and such acoustic modes can exist even in the absence of gravity, hence the label *S* (for "sound"). *S* modes are found to be strongly dispersed, mainly due to the irregular variation in sound velocity with height, a property physically equivalent to the dispersion of seismic Rayleigh waves in a layered Earth.

By contrast, the *GR* modes exist only for a gravitating model (Harkrider & Press, 1967, p. 153) in which the restoring force is, as least partially as we will show, of a gravitational nature, hence the *GR* label. These modes, especially the fundamental branch GR_0 (Harkrider, 1964), exhibit very little dispersion at frequencies lower than the Brunt–

Väisälä frequency f_{BV} (also known as the buoyancy frequency), which characterizes the bobbing of an atmospheric particle displaced vertically and adiabatically in a stable atmosphere (Väisälä, 1925; Brunt, 1927):

$$f_{BV}^2 = -\frac{g}{4\,\pi^2}\left(\frac{1}{\rho}\frac{d\,\rho}{dz} + \frac{g}{\alpha^2}\right) \tag{1}$$

where g is the local acceleration of gravity at altitude z, ρ the local density, and α the local sound velocity.

Note that the actual value of the Brunt–Väisälä frequency in the atmosphere remains to this day controversial. L10 (p. 543) quotes a value of 5 min for the period T_{BV} while several textbooks advocate about double [e.g., 10 min (Gill, 1982, p. 52); 8 min (Holton, 2004, p. 54)]. Its value for an isothermal atmosphere at 288 K is 343 s or 5.7 min. In the ARDC model, the Brunt–Väisälä period T_{BV} is close to 7 min at the bottom of the atmosphere, features a minimum of 5.5 min around 80 km, and then rises to 10 min at $z = 125$ km. This would suggest that the discrepancy between published estimates may be due to modeling at various altitudes by different authors. To our best knowledge, the only experimental measurement of T_{BV} was obtained from the resonant frequencies of surface waves excited by the 1991 Pinatubo explosion (Kanamori et al., 1994) which yielded $T_{ac} = 275$ s = 4.6 min for the acoustic cutoff period, suggesting $T_{BV} = 305$ s ≈ 5 min given the theoretical ratio $(\gamma/(2\sqrt{\gamma-1}))$ of the two periods in an isothermal atmosphere. Preliminary results from the 2022 Tonga explosion would tend to confirm these experimental values.

Theoretical phase and group velocities for the GR_0 mode below f_{BV} are typically on the order of 315 m/s (e.g., Press & Harkrider, 1962), which clearly identifies the branch as the "Lamb wave", and agrees with values observed for air waves generated by the Tonga explosion (e.g., Gusman et al., 2022; Okal, 2022). Intense coupling between *S* and *GR* modes takes place around f_{BV}.

In this general framework, Press and Harkrider (1962) and Harkrider (1964) described the *GR* modes as gravitational oscillations of a fluid layer (the atmosphere) bounded by a free surface at its top (where, in the ARDC model, the density ρ and bulk modulus K_S have decreased by factors of $\sim 10^8$ at an

---

[1] The interpretation of these early papers is occasionally made difficult by the then customary use of the word "tidal waves" to describe tsunamis, i.e., gravitational oscillations of an oceanic mass which we now understand have nothing to do with tides.

altitude of 130 km), and, in the absence of an ocean, an essentially rigid boundary at the bottom, where ρ jumps by a factor of about 3000 and K_S by more than 10^5 (in the presence of an ocean, ρ would still jump by a factor of 1000 and K_S by 10^4). This model is conceptually reminiscent of that of the tsunami of an oceanic layer, and this similarity begs the question whether the GR modes can be interpreted physically as the "tsunamis" of the atmosphere, the word "tsunami" being taken to mean a wave propagating in a fluid layer and featuring an oscillation between kinetic and gravitational energy.

In particular, in such a context, the undispersed nature of the GR_0 branch in the low-frequency limit would suggest that it satisfies the long-wave or "Shallow-Water" approximation [hereafter SWA]. Given that the acceleration of gravity, g, varies only minimally, from 9.81 to 9.40 m/s^2 through the 130 km of the model used here, we find that the SWA interpretation of its constant celerity $C \approx 315$ m/s would lead to an effective height

$$H_{eff} = C^2/g = 10.0 \text{ to } 10.4 \text{ km.} \qquad (2)$$

In the case of an atmosphere whose properties, in particular its density, vary strongly with altitude, it is impossible to define a priori its thickness, but this figure (10.2 km on the average) appears reasonable as an order of magnitude.

Indeed, using the ARDC model, we note that at the altitude $H_{eff} = 10$ km, the density is reduced by a factor 3.2, and that the first 10 km of atmosphere contribute 78% of the pressure at the solid surface. More generally, Fig. 1a documents the decay of density ρ with altitude. Because of the small thickness of the dense atmosphere (~ 10 km), and to make the figure more legible, we use a variable horizontal scale in this figure and several subsequent ones: the scale is linear but different in the solid Earth, between altitudes of 0 and 10 km, and above 10 km. The density ρ, scaled to that at the lower boundary of the atmosphere ($\rho_0 = 1.224$ kg/m^3) is plotted using a logarithmic scale. It decreases by about 8 orders of magnitude from bottom to top of the model, but this decay differs in the lower and upper bands. From 0 to 10 km, $\log_{10} \rho$ varies with a slope of -0.047 logarithmic units per km, vs. -0.068 between 10 and 130 km. Yet another approach would be to compute the altitude of the center of mass

of the atmosphere, which is found at 7.2 km in the flat-layered ARDC model, suggesting a value of 14.4 km for its "thickness". All these remarks support a value of 10 km as a general order of magnitude of H_{eff}. Finally, we verify that at periods of ~ 1000 s and with $C = 315$ m/s, the proposed thickness $H_{eff} \approx 10$ km is indeed much shorter than a typical wavelength (315 km), which justifies the use of the SWA.

This general concept of an intrinsic similarity between atmospheric air waves and the tsunamis of an oceanic layer is indeed found in the early works of e.g., L10 or Pekeris (1937). In particular, L10 argued, in the general footsteps of Laplace (1805), that the so-called "longitudinal wave" was indeed of the same nature as oceanic gravitational oscillations (which we would nowadays call "tsunamis"), for a "virtual height" H (in his notation) which L10 estimated at the slightly lower value of 27,640 ft. or 8.4 km.

These remarks bring a quantitative legitimacy to the possibility that GR waves could be interpreted as the "tsunamis" of the atmosphere. This question constitutes the subject of this study, which will reach a *negative* conclusion, by focusing on a systematic investigation of the physical nature of the potential energy exchanged with kinetic energy during their propagation.

Finally, we note that Pekeris (1939) detailed properties of higher-order solutions to the dispersion equations; because their phase velocities are less than those of the fundamental GR_0, they should properly be called *undertones*. Harkrider and Press (1967) showed that the second undertone GR_2 can be effectively coupled to the oceanic layer and thus contribute to marigrams in the far field. More recently, Watanabe et al. (2022) have described their systematic recording following the Tonga explosion and proposed the name "Pekeris wave" for the GR_2 branch, in parallel to the "Lamb wave" descriptor generally used for GR_0.

2. Modeling the GR_0 Branch

In this section, we consider the ARDC atmospheric model, coupled to the solid Earth PREM structure (Dziewonski & Anderson, 1981), with no oceanic layer. In practice, and to facilitate some

computations, we truncate the model at an altitude of 130 km (see Fig. 1), where the density of the atmosphere has decreased by a factor of about 10^8 from its value at the Earth's surface. In addition to the density ρ plotted on Fig. 1a, Fig. 1b similarly shows the compressional velocity α (speed of sound) scaled to the undispersed celerity of the GR_0 mode at low frequencies, $C = 315$ m/s. While exhibiting significant fluctuations, α varies only by a factor of about two between its minimum (258 m/s at 85 km), and its maximum (556 m/s at the top of the model). Under the assumption that the atmosphere is a perfect gas, this corresponds to a factor of only 4 in absolute temperature Θ, which justifies the isothermal models used by some authors (e.g., Kanamori et al., 1994; Laplace, 1805; L10).[2]

We then compute GR modes as a particular case of the spheroidal modes of the Earth, for a model including a realistic atmosphere, with or without an oceanic layer. The general approach for such computations of normal modes was given by Saito (1967) and implemented in a routine fashion by many authors, e.g., Kanamori and Cipar (1974). Their algorithm represents the eigenfunction of the mode as a 6-dimensional vector y_i whose components are detailed in Appendix 1.

In a landmark study, Ward (1980) showed that oceanic tsunamis could be described as a particular branch of spheroidal modes, when the Earth model includes an oceanic layer. The power of this approach resides in its ability to automatically solve all problems of coupling at the ocean-solid Earth interface, including the effect of any sedimentary layers (Okal, 1982, 1988). Later, and largely motivated by the 1991 Pinatubo eruption, the method was extended to include atmospheric layers (Lognonné et al., 1998).

An alternative approach is Harkrider's (1964) algorithm, based on a Haskell-Thomson propagator (Haskell, 1953), and written in the framework of a flat-layered two-dimensional structure composed of the atmosphere, a possible oceanic column, and a solid Earth. We have verified that the two approaches give similar results. We note however that Harkrider and Press (1967) use the simplifying assumption $\gamma =$
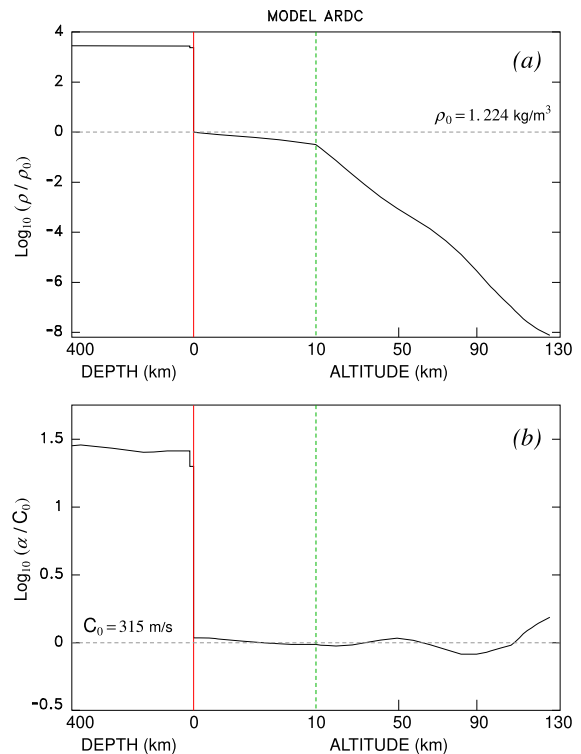
---

[2] Throughout this paper, we use Θ for absolute temperature, to distinguish it from periods T.

Figure 1

a Particle density ρ as a function of depth (or altitude) for Model ARDC. The density is scaled to its value at the bottom of the atmosphere, $\rho_0 = 1.224\,\text{kg/m}^3$, shown as the grey horizontal dashed line, and plotted on a logarithmic scale. Depth into the solid Earth and altitude into the atmosphere are plotted linearly, but with different scales in the solid Earth (to the left of the red line), in the lower atmosphere (the first 10 km), and above 10 km (to right of the green dashed line). **b** Sound velocity α in the ARDC model, scaled to the observed celerity of the GR_0 branch, $C = 315$ m/s, shown as the grey horizontal dashed line

---

1 for the classical heat capacities ratio, except in the calculation of the Brunt–Väisälä frequency as a function of altitude.

We first analyze in some detail the eigenfunction of the GR_0 wave in the absence of an ocean, at a period T close to 1000 s, by solving the free oscillation of the structure at an angular degree $l = 127$. Figure 2a shows the variation of the vertical particle motion, y_1 in the notation of Saito (1967) and Kanamori and Cipar (1974), scaled to its value at the bottom of the atmosphere, and using the same plotting conventions as in Fig. 1. After a rapid growth by 4 orders of magnitude in the first 2 km of the atmosphere, it remains practically constant in the next
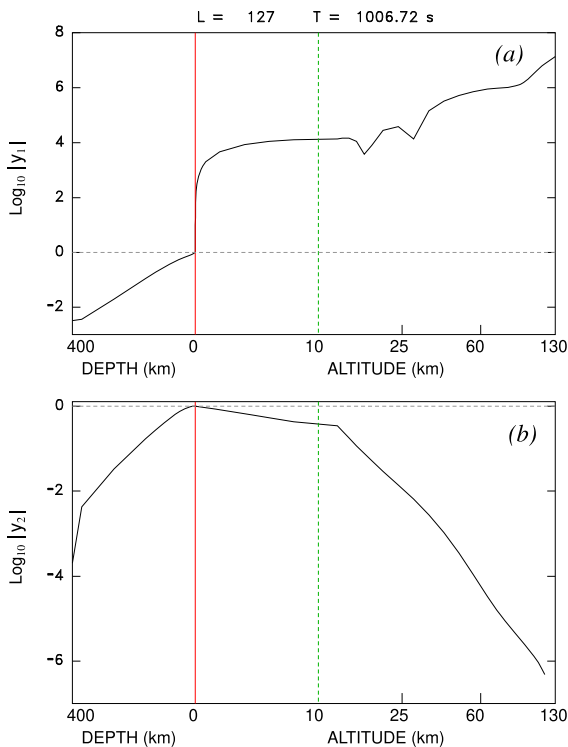
Figure 2

Eigenfunction of the mode GR_0 computed at a period $T \approx 1000$ s. **a** Vertical particle motion y_1, scaled to its value at the bottom of the atmosphere, and plotted on a logarithmic scale. Plotting conventions as in Fig. 1. Note the growth by about 4 orders of magnitude between the first 10 km of the structure (dense atmosphere) and its top (rarefied atmosphere). The two irregularities around 30 km represent changes of sign in y_1. **b** Same as **a** for the stress y_2 (opposite of the overpressure in the atmosphere), scaled to its value at the Earth's surface. Note the more regular decay by 6 orders of magnitude to the top of the atmosphere

10 km, and then increases regularly by about 3 more orders of magnitude at the top of the model considered. Such large values of particle motion simply express the rarefaction of the atmosphere whose density has, by then, fallen by 8 orders of magnitude (see Fig. 1a): the wave imposes considerable displacements, but only on microscopic masses of air. Between ~ 25 and 50 km, the eigenfunction y_1 has nodes and changes sign twice, hence the artificial irregularities in the logarithmic plot, which mandates the use of its absolute value. By contrast, the particle motion y_1 simply decreases exponentially—linearly using a logarithmic scale—inside the solid Earth.

A simpler insight into the structure of the eigenfunction can be gleaned from its component y_2 representing the radial stress σ_{rr}, shown in Fig. 2b, and which in fluid layers is simply the opposite of the overpressure during the oscillation. It is found to be maximum at the boundary between solid Earth and atmosphere, and to decrease more regularly with altitude (or depth in the solid Earth), losing about 6 orders of magnitude from the bottom of the atmosphere to the top of the model at 130 km. In this respect, y_2 appears as a more rational physical descriptor of the eigenfunction than the vertical displacement y_1.

On Fig. 3, we take a detailed look at the structure of the eigenfunction in the first 20 km of the atmosphere, and especially in the first 10, which reveals significant departures from that of a classical tsunami under the SWA. The vertical displacement $y_1(z)$, scaled to its value at 10 km, is found to rise sharply in the first few km of the structure, and hence depart from the linear dependence predicted under the SWA (dashed line on Fig. 3a). This behavior is totally robust when the frequency of the wave is changed in the domain where the GR_0 wave is not dispersed (red, black and green lines for $T \approx 2000$, 1000 and 640 s, respectively; note that they all plot essentially on top of each other). Similarly, the horizontal displacement, $l y_3$ in Saito's (1967) formalism (see Appendix 1), would be expected to be constant throughout the column under the SWA, but is found to increase slightly with altitude (solid lines with same color code on Fig. 3b), this deviation being more pronounced at lower frequencies. Such deviations from the SWA model for a homogeneous liquid layer result from the density layering in the atmosphere. However, and most remarkably, the strongest deviation from that model occurs in the ratio $(l y_3 / y_1)$ which characterizes the ellipticity of the particle displacement, and in particular the aspect ratio of the surface motion when computed at the top of an oceanic layer of thickness $H_{Oc.}$. Under the SWA, it is expected to take the classical value (e.g., Dean & Dalrymple, 2000, Chap. 4):

$$\frac{l y_3}{y_1^{Top}} = \frac{C}{\omega H_{Oc.}} = \frac{\sqrt{g}\, T}{2\pi \sqrt{H_{Oc.}}} \qquad (3)$$
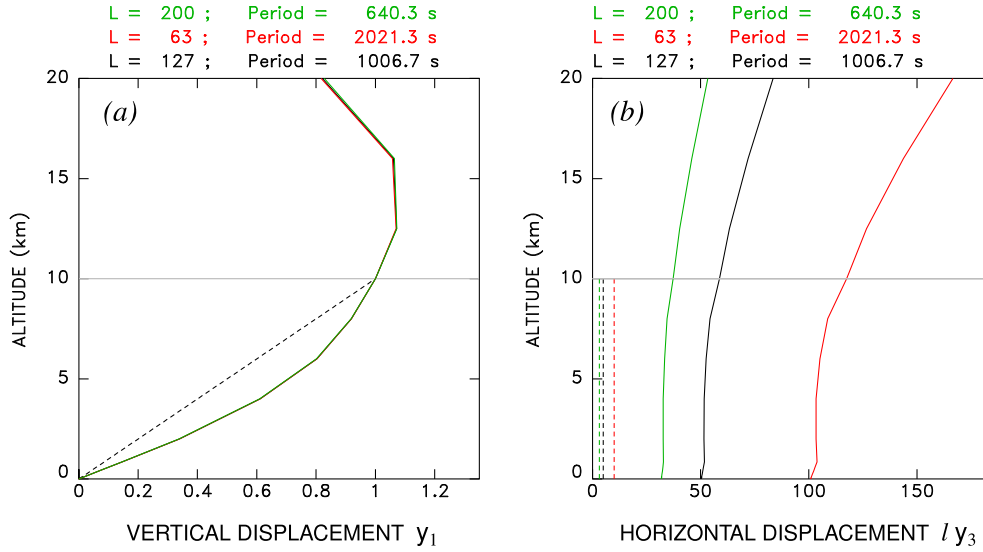
L = 200 ;   Period =   640.3 s
L =   63 ;   Period =   2021.3 s
L = 127 ;   Period =   1006.7 s

Figure 3

a Close-up of the structure of the vertical displacement y_1 of the eigenfunction of the GR_0 branch in the bottom 20 km of the atmosphere, normalized to its value at 10 km (grey horizontal line), at periods close to 1000 s (black), 2000 s (red) and 640 s (green). Note that the three curves plot essentially on top of each other. The dashed straight line is the linear dependence expected under the SWA for a classical tsunami. Note the faster growth of y_1 with altitude for the air wave in the deepest (and densest) layers. **b** Same as **a** for the horizontal component $(l\,y_3)$, also normalized to $y_1 = 1$ at 10 km. The vertical dashed lines are the constant values expected under the SWA. Note the much larger values of $(l\,y_3)$ for the air wave

As shown on Fig. 3b, this discrepancy reaches a factor of 11.7, which is remarkably constant at the three frequencies tested (~ 0.5, 1, 1.5 mHz). Reconciling this discrepancy would require dividing the effective thickness of the atmosphere by more than 100, which is obviously totally unrealistic since its properties have hardly changed at an altitude of 100 m. Our results thus underscore a significant deviation of the structure of GR_0 from that of a genuine tsunami.

The computation most fundamental to our discussion is that of the energy of the oscillation. Expressions for the kinetic and potential energies in the oscillation, E_K and E_P, are given, e.g., by Wiggins (1976, pp. 143–144). In its potential form E_P, the energy is itself the sum of an elastic component E_E and a gravitational one E_G. In the case of a fluid column ($\mu = 0$), these can easily be separated from the various integrals I_{si} ($i = 3, 4, \ldots, 12$) listed by Wiggins:

$$E_K = \omega^2 \int_0^{r_{max}} \rho\, r^2 \left[y_1^2 + l(l+1)\, y_3^2 \right] \cdot dr \quad (4a)$$
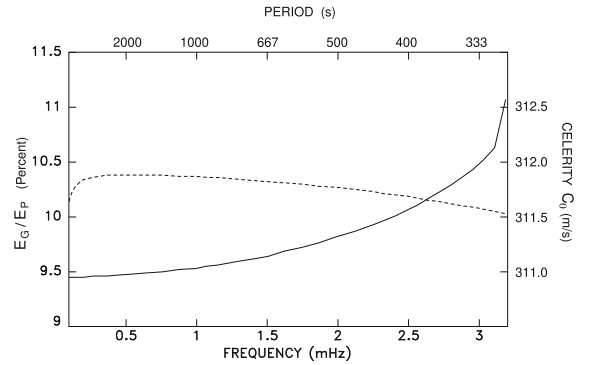

Figure 4

Fraction of gravitational energy E_G in the potential energy as a function of frequency along the GR_0 branch (solid line; left scale in percent). Note that it increases only slowly, until the frequency reaches the domain of coupling with S modes near the Brunt–Väisälä frequency. The phase velocity of the wave is also very stable, varying by no more than 0.12% over the same frequency range (dashed line, scale at right)

$$E_P = E_E + E_G \quad (4b)$$

$$E_E = \int_0^{r_{max}} K \left[(r\, y_1' + 2\, y_1) - l(l+1)\, y_3 \right]^2 \cdot dr \quad (4c)$$
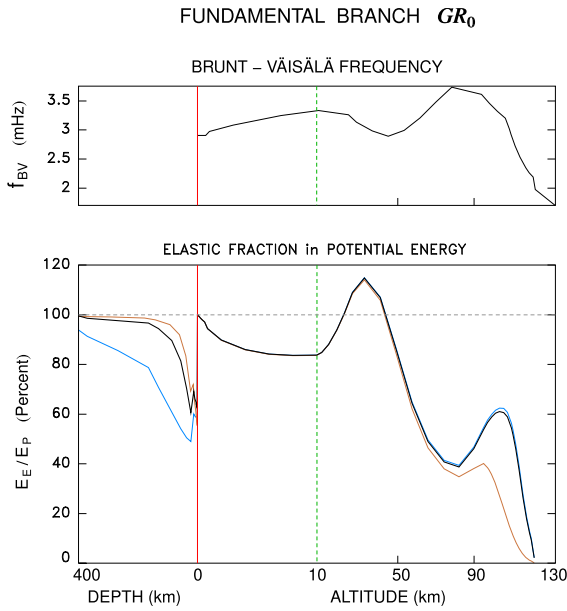
Figure 5

The *bottom* frame shows the ratio of in situ kernels of elastic and total potential energy as a function of depth, during the oscillation of a GR_0 mode at $T \approx 1000$ s (thick black curve). Plotting conventions as in Fig. 1. Note the generally high ($> 80\%$) fraction of elastic energy, except in the most rarefied sections of the atmosphere. The robustness of these results is confirmed by superimposed plots at $T \approx 3000$ s (blue line) and 480 s (beige line). Note the systematic occurrence of values in excess of 100% around 24–43 km (see text for discussion). The *top* frame plots the in situ Brunt–Väisälä frequency as a function of depth

$$E_G = \int_0^{r_{max}} \left[4\pi G\, \rho\, r^2\, y_1^2 - 2\rho\, ry_1 \left(2gy_1 + ry_5'\right) \right.$$
$$+ 2\, l(l+1)\, r\rho\, y_3 \left(gy_1 - y_5\right)$$
$$\left. + \frac{1}{4\pi G} \left[(l+1)\, y_5 + ry_5' \right]^2 \right] \cdot dr$$

$$(4d)$$

where K is the bulk modulus, the prime indicates a derivative with respect to the radius vector r, and the eigenfunction components are in the notation of Saito (1967). Incidentally, the identity $E_K = E_E + E_G$ can serve as a quality check for the numerical computation of the mode. We generally achieved a 99.9% fit to this equation.

For the mode initially targeted ($l = 127$; $T \approx 1007$ s), we find that E_E accounts for 90.5% of E_P, and E_G for only 9.5%. In other words, the potential energy of the wave is overwhelmingly elastic, thus largely negating the concept of GR_0 being a "gravity wave". On Fig. 4, we show that this result is totally robust across the large frequency band where the GR_0 branch is undispersed (from 0.10 to 3 mHz; $l = 12$ to 410). This result is a direct consequence of the departure of the aspect ratio of particle motion ($l\, y_3/y_1$) from its value for a genuine tsunami (see Fig. 3). As shown in Eq. (4), an increase in y_3 will contribute a linear change to the gravitational energy E_G but a quadratic one to both its elastic and kinetic counterparts, E_E and E_K, thus *increasing* the proportion of elastic energy in E_P.

Only when the frequency approaches its Brunt–Väisälä value (about 2.9 mHz in the lower, denser atmosphere), does the fraction E_G/E_P start growing above 10%. Meanwhile, the phase velocity (dashed line on Fig. 3) remains remarkably constant, decreasing by only 0.2 m/s or 0.07% in the frequency band considered.

On Fig. 5, we further examine the variation of the ratio of the kernels of E_E and E_P as a function of altitude in the atmospheric column (or depth inside the solid Earth). They are simply the integrands in the various lines of (4). We find that this ratio remains very high (greater than 80%) throughout most of the atmospheric column; it falls below that value only when the medium becomes rarefied (above 50 km, where the density has fallen by a factor of 1000). This means that most of the mass of the atmosphere oscillates by exchanging kinetic energy with *elastic* energy, the contribution of gravity remaining rather marginal. Only in the uppermost part of the structure ($z > 100$ km) does the potential energy become primarily gravitational. We also present results at periods of 3000 and 480 s, respectively, which share these characteristics.

An interesting point is that the kernel ratio E_E/E_P becomes greater than 1 at altitudes $z = 24$ to 43 km; this means that the gravitational potential energy becomes *negative*, which could appear paradoxical at first sight. However, as outlined by Dahlen and Tromp (1998, p. 295), a similar situation takes place for the Earth's seismic radial modes. We have
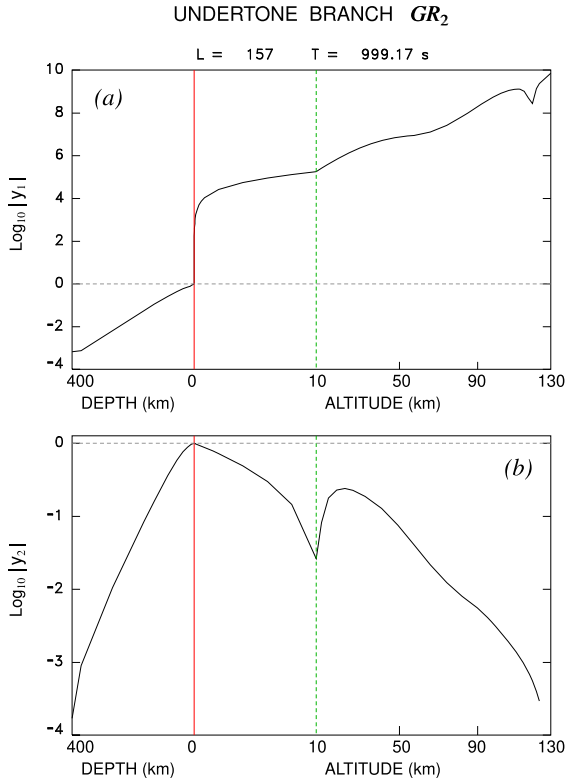
Figure 6

Same as Fig. 2 in the case of the undertone "Pekeris" mode GR_2 at $T \approx 1000$ s. Note the faster and smoother growth of y_1 with height, and the more complex behavior of y_2

Figure 7
Same as Fig. 5 for the undertone GR_2

verified, for example that the ratio E_E/E_P is 132% for the fundamental radial mode $_0S_0$ and 111% for its first overtone $_1S_0$. The physical explanation, incidentally qualified as "obvious" by Dahlen and Tromp (1998), would be that E_G can become negative under a trend towards a gravitational collapse (which remains controlled in the case of a stable atmosphere featuring a real Brunt–Väisälä frequency, or in the case of the radial modes of the Earth by a sufficient elasticity, albeit weak in the absence of transverse stresses). Equation (4d) shows that this effect is due analytically to crossover terms of the form $(y_1 \, y_3)$, as opposed to strictly quadratic ones in (4a) and (4c).

Note in particular that E_G becomes negative in the general band of altitudes where the vertical motion y_1 has nodes, and changes sign (25–50 km). It is remarkable that this is also the zone of a local minimum in the value of the in situ Brunt–Väisälä frequency f_{BV}, as shown on the top frame of Fig. 5. In
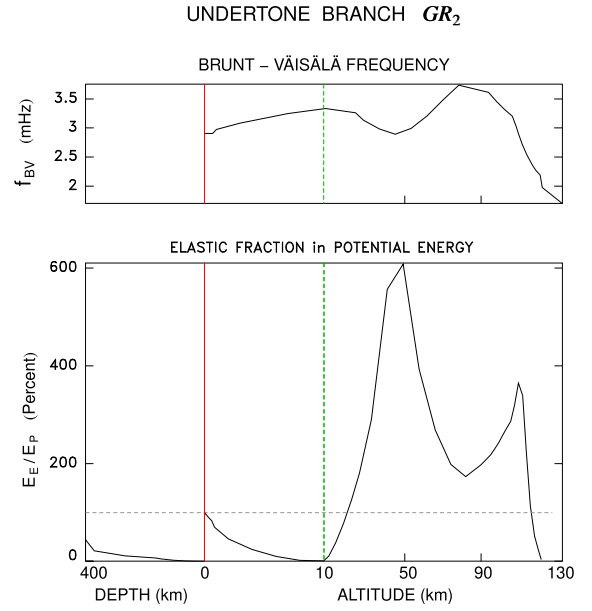
general, a low f_{BV} will express a less efficient gravitational restoring force for a given vertical displacement (it would disappear for $f_{BV} = 0$). Indeed, we find a significant, if not wholly perfect, anti-correlation of -79% between the kernel ratio E_E/E_P and f_{BV} in the depth range 26–89 km.

The conclusion of this section is that, contrary to a widespread perception, the GR_0 branch is not in the nature of gravitational oscillations, since the energy of the restoring forces is overwhelmingly of an elastic nature, at least throughout the denser layers of the atmospheric column, where the oscillation actually moves significant masses of air. In other words, a "putative tsunami" of the atmosphere is subject to coupling with the elastic properties of the medium, to the extent that the physical nature of the wave is changed. It can then be assumed that the origin of this coupling resides in the similarity of the undispersed celerity of the would-be "atmospheric tsunami" (313 m/s) and the intrinsic speed of sound in the denser layers of the atmosphere comprising most of its mass (~ 340 m/s). Note that this concept was inherent in the efforts of the early authors on this subject (L10; Pekeris, 1937; Taylor, 1937). Section 3 will explore this assumption by examining in detail

the effect of the speed of sound α on the physical nature of a conventional tsunami wave in the ocean.

Finally, we examine the case of the "Pekeris" undertone GR_2 which Harkrider and Press (1967; Fig. 8) have shown can make a weaker but significant contribution to the far-field overpressure (and sea level disturbance in the presence of an oceanic column). In the low-frequency limit, this wave has a celerity of ~ 260 m/s, intermediate between those of GR_0 (313 m/s) and of a tsunami wave in a 5-km deep ocean (220 m/s). Figure 6 is a counterpart to Fig. 2 at a period of ~ 1000 s, the corresponding degree for a GR_2 mode being $l = 157$. The vertical displacement y_1 is found to increase even faster with height in the atmosphere, gaining 10 orders of magnitude to the top of the structure, but more regularly, with only one change of polarity around 120 km. By contrast, the stress y_2 (opposite of the overpressure) decreases slower than its fundamental analog, and features a change of sign around $z = 10$ km. On Fig. 7, the ratio of the kernels of E_E and E_P is shown to be much larger than 1 over a major part of the atmosphere, to the extent that the

integrated value for the whole mode, 155%, is itself greater than 1. In this respect, this undertone also features very significant elastic deformation and neither can it be regarded as a "tsunami" of the atmosphere.

3. A New Look at the Effects of Elasticity and Layering on an Oceanic Tsunami

We revert here to the case of the classical tsunami of an oceanic layer, bounded by a realistic model of the Earth (e.g., the PREM model) and a free surface with no atmosphere. We explore the effect of large variations in compressibility, and hence speed of sound α in the ocean, on the nature of the eigenfunction of the tsunami, and in particular on the distribution of potential energy between its elastic and gravitational forms.

The question of the influence of elasticity on the dispersion of a standard tsunami was investigated more than 40 years ago by Okal (1982), who used the spheroidal mode approach (Ward, 1980) to obtain a
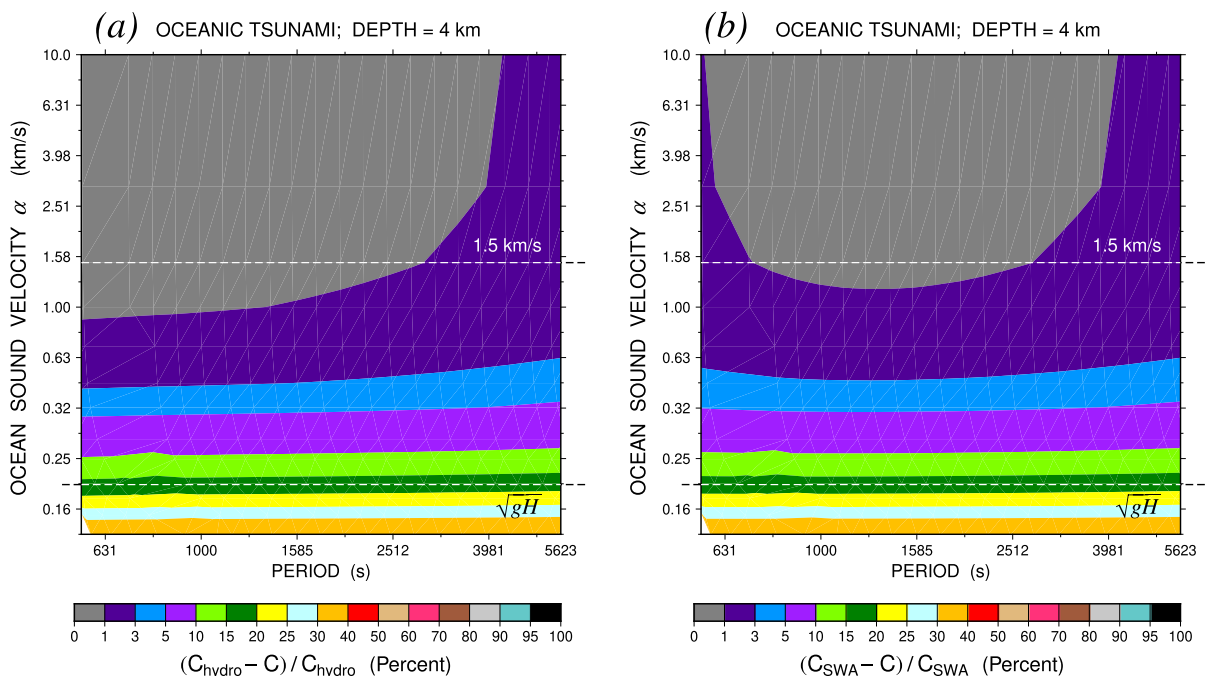

Figure 8

Deviation of the phase velocity C of the tsunami of a 4-km oceanic column contoured as a function of period and sound velocity in the ocean. Both scales are logarithmic. On the left frame (**a**), the reference velocity is C_{hydro} defined by Eq. (3); on the right one (**b**), it is simply its value under the SWA. The dashed lines indicate a realistic value of α (1.5 km/s) and for reference $C_{SWA} = \sqrt{g H_{Oc.}} = 198$ m/s
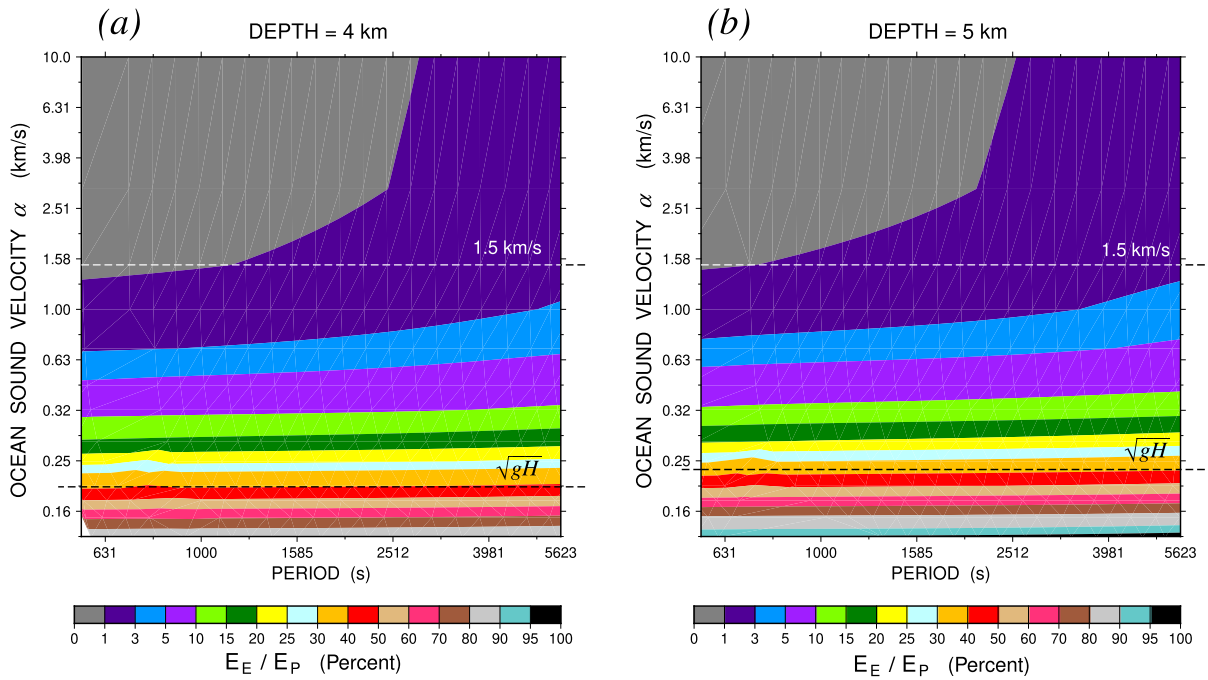
Figure 9

a Ratio of elastic to total potential energy, E_E/E_P, in the classic tsunami of a 4-km deep ocean, contoured as a function of period T and sound velocity α (using logarithmic scales). The ratio remains less than 2% at all periods for a realistic value of α (1.5 km/s), but would increase significantly for much smaller α. **b** Same as **a** for a 5-km deep ocean

reduction of phase velocity $\delta C/C \approx -C^2/6\alpha^2$, on the order of -0.3% (or -1.5 m/s) in a 4-km deep ocean at a typical period of 1000 s, and for a realistic value of the speed of sound in seawater (1.5 km/s). Indeed, subtle discrepancies had been reported as early as 60 years ago (Nakamura & Watanabe, 1961) between arrival times of recorded tsunamis and simulated waveforms, and such observations were later confirmed systematically on the high seas, using ocean-bottom DART sensors (e.g., Hébert *et al.,* 2009; Rabinovich *et al.,* 2011). Motivated by such reports, several authors, notably Watada et al. (2014) and Abdolali and Kirby (2017), showed that they were a combined effect of the finite compressibility of the ocean, as well as of the gravitational oscillation of the solid Earth below it, two agents not included in traditional simulation algorithms, e.g., MOST (Titov et al., 2016), which assume a rigid bottom and an incompressible ocean. We note of course that Ward's (1980) approach using a normal mode algorithm in Saito's (1967) full 6–dimensional formalism automatically accounts for both.

However, as those authors were motivated by observations in the real ocean, they limited their investigations to realistic values of α (about 1.5 km/s). On the other hand, Okal (1982) investigated a wider domain of values of α, but restricted his study to $l = 200$, in practice $T \approx 1000$ s. In order to gain a more profound understanding of the coupling between elasticity and gravity, we will explore this question over a broad range of values of both T (from 600 to 6000 s), and α (from 10 km/s down to 125 m/s), such extreme sound velocities being clearly irrelevant in a real-life ocean, but the lower ones providing insight for an application to the atmosphere. We fix the depth of the oceanic column at $H_{Oc.} = 4$ km, to allow direct comparison with the works of Okal (1982) and Watada et al. (2014).

On Fig. 8a, we contour the opposite of the deviation, expressed in percent, of the phase velocity C from its value C_{hydro} in a hydrodynamic model taking into account its dispersion outside the SWA, but neglecting the elasticity of the ocean and the elastic

and gravitational properties of the solid Earth. C_{hydro} is calculated numerically at each frequency from

$$\omega = C_{hydro}\, k_{hydro} \quad \text{and}$$
$$\omega^2 = g\, k_{hydro}\, \tanh\left(k_{hydro}\, H_{Oc.}\right). \tag{5}$$

The figure uses logarithmic scales for period T and sound velocity α. Figure 8b similarly contours the absolute value of the deviation of C with respect to its value under the SWA, routinely used in transoceanic simulations. Finally, on Fig. 9, we contour the elastic fraction of the potential energy, E_E/E_P, also expressed in percent, as a function of α and T.

As expected, the primary difference between Figs. 8a and 8b takes place at shorter periods where the SWA starts to break down, and C_{hydro} becomes smaller than C_{SWA}. However, that effect is limited to larger (and realistic) values of α. As α becomes smaller, its effect dwarfs that of the breakdown of the SWA. For $\alpha = 1.5$ km/s, we confirm the general patterns identified by Watada et al. (2014), who found a minimum reduction of celerity of $\sim 1\%$ with respect to the SWA value around 1000 s (their Fig. 5a). The intrinsic contribution of α is more important at longer periods, but the breakdown of the SWA takes over at the shorter ones. In this respect, it was unfortunate that Okal (1982) inadvertently restricted his study to $l = 200$ (in practice $T \approx 1000$ s, precisely the locus of the minimum), which led him to conclude that the effect of finite α was essentially negligible; note also that Okal (1982) did not consider the breakdown of the SWA.

On Fig. 9a, we similarly contour the ratio E_E/E_P of elastic to total potential energy of the oceanic tsunami. The general shape of the figure is remarkably similar to that of Fig. 8a, but the ratio grows significantly faster with decreasing α. In the vicinity of $T = 1000$ s, we reproduce the results of Okal (1982, Table 1), who obtained ratios of $\sim 1\%$ for $\alpha = 1.5$ km/s and 38% for $\alpha = 200$ m/s, essentially equal to the SWA celerity for $H_{Oc.} = 4$ km (198 m/s), and shown as the lower white dashed line on Fig. 9a. On Fig. 9b, we extend the investigation to a deeper oceanic column ($H_{Oc.} = 5$ km), and find that the potential energy grows even faster with decreasing α, reaching 50% at 200 m/s; however, E_E/E_P keeps the same value ($\sim 37\%$) at the SWA celerity (now faster
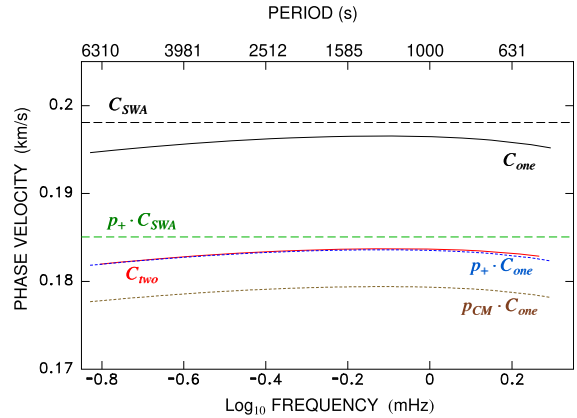

Figure 10

Comparison of the tsunami dispersion of one- and two-layer 4-km deep oceans. The thin black line is the phase velocity C_{one} of the one-layer (homogeneous) model with the reference SWA value shown as the black dashed line. The green dashed line results from the application of the correction p_+ (6) to the SWA value, and the dotted blue trace to C_{one}. The thick red line is the dispersion C_{two} computed for the 2-layer model detailed in the text; note the perfect agreement with ($p_+ \cdot C_{one}$). The brown dotted line results from applying the correction $p_{CM} = 0.913$ to C_{one}

at 221 m/s). Indeed, we have verified the robustness of this ratio for unrealistically deep oceans, all the way to $H_{Oc.} = 230$ km, where the SWA tsunami celerity reaches the classic sound velocity in seawater (1.5 km/s). Finally, our more systematic investigation across a wide frequency band shows that E_E/E_P becomes largely independent of frequency for $\alpha < 500$ m/s.

As the elastic fraction in the potential energy reaches such ratios, and further increases for even lower α, the physical nature of the oscillation in the wave is fundamentally altered. A ratio of 25% elastic energy can be regarded as a threshold beyond which the wave is no longer of a gravitational nature and ceases to be a legitimate "tsunami" (Okal, 1982).

An additional issue, not taken into account in the above computations, nor in Okal (1982), is that in the presence of gravity, a finite compressibility of the fluid will result in an increase of its density ρ with depth in the ocean. This additional effect on the celerity of a standard oceanic tsunami was examined by Tsai et al. (2013), who showed that an increase of density with depth in the oceanic column leads to a decrease of celerity, on the order of an additional 0.5% under the SWA for realistic models of the ocean
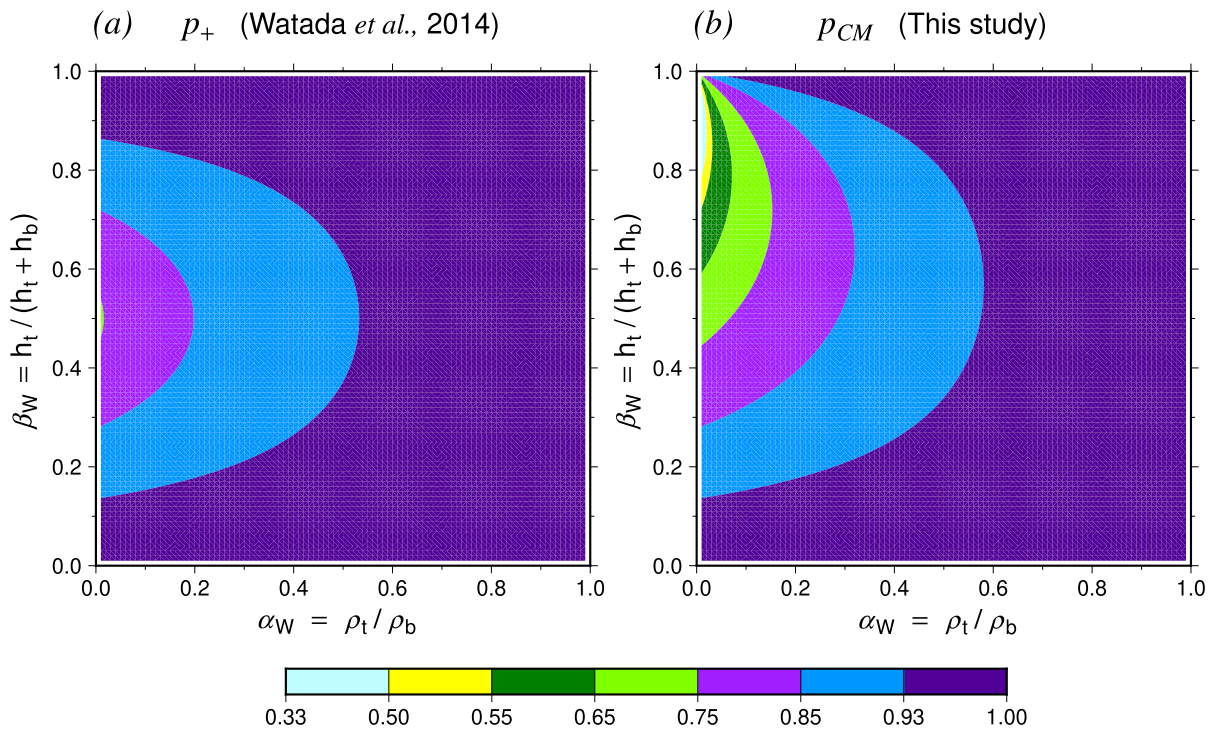
(a) p_+ (Watada *et al.*, 2014)   *(b)* p_{CM} (This study)

Figure 11

a Values of the correction p_+ derived under the SWA by Watada et al. (2014) for the tsunami of a two-layer 4-km deep ocean, contoured for the full range of parameters α_W and β_W characterizing the layering. **b** Same as **a** for the parameter p_{CM} using the simplified Center-of-Mass approach. Note the general agreement of the two parameters, except for very small values of α_W and very large ones of β_W

(i.e., a linear increase in ρ of 0.8% or 8.6 kg/m^3 from top to bottom). Watada (2013) later considered the formal case of a two-layer incompressible ocean and derived an exact formula for the correction of its tsunami celerity [his Eq. (36) p. 4004]:

$$\frac{C^2_{two}}{C^2_{one}} = p_+^2$$
$$= \frac{1}{2}\left[1 + \sqrt{1 - 4(1 - \alpha_W)(1 - \beta_W)\beta_W}\right] \qquad (6)$$

where $\alpha_W = \rho_t/\rho_b$ and $\beta_W = d_t/(d_t + d_b)$ are dimensionless ratios relating the densities and thicknesses of the top (t) and bottom (b) layers (we add a subscript W to α and β, to distinguish them from the sound velocity, α in our notation, and from the parameter β introduced by L10; see Sect. 4 and Appendix 2).

Because once again, these authors were largely motivated by an application to real oceans, they focused primarily on small variations in ρ, which
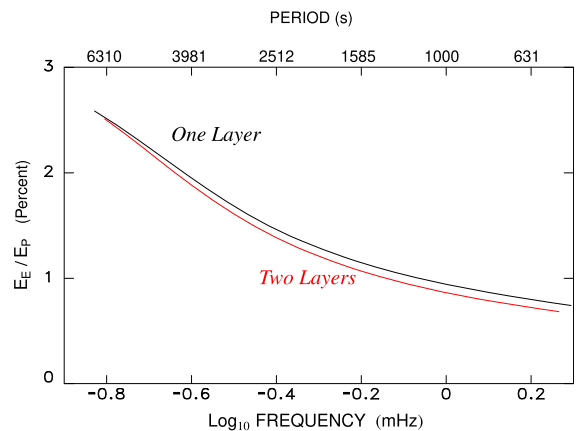

Figure 12

Elastic fraction E_E/E_P of the potential energy for tsunami modes of a 4-km deep ocean, computed for a single-layer homogeneous ocean (black line), and a two-layer one (red line) with a 1:2 density contrast ($\alpha_W = 1/2$) and a 2:1 thickness ratio ($\beta_W = 2/3$). Note the minimal difference between the values, across the whole frequency spectrum

Table 1

Results of modeling of GR_0 for various values of ϕ

Models (Sects. 4 and 5.1)							Numerical simulations (Sect. 5.2)					
ϕ	m	ζ (km)	β (K/km)	α_ϕ (km/s)	C_ϕ (km/s)	α_ϕ/C_ϕ	C (km/s)	C/α_ϕ	C/C_ϕ	ξ	TEST	E_E/IE_P (%)
	(47)	(16)	(45)	(26)	(24)					(36)	(37)	
1.000	∞	∞[a]		0.339	0.406	0.835	0.339	1.000	0.835	∞		96.4
1.032[b]	31.250	270.9[a]	1.063	0.334	0.400	0.835	0.329	0.985	0.823	28.4026	1.005	84.6
1.050	20.000	176.4[a]	1.633	0.332	0.397	0.836	0.325	0.979	0.819	18.1016	1.000	80.4
1.065	15.385	137.6[a]	2.093	0.330	0.394	0.838	0.322	0.976	0.816	13.8689	1.003	78.0
1.080	12.500	113.4	2.540	0.328	0.392	0.837	0.319	0.973	0.814	11.1775	1.000	75.1
1.100	10.000	92.4	3.117	0.325	0.389	0.835	0.315	0.970	0.810	8.8488	1.004	72.2
1.150	6.667	64.4	4.472	0.319	0.382	0.835	0.308	0.966	0.807	5.6314	1.002	66.5
1.167	6.000	58.8	4.898	0.317	0.380	0.834	0.306	0.965	0.806	4.9640	1.001	65.5
1.200	5.000	50.4	5.714	0.314	0.376	0.835	0.302	0.962	0.804	3.9356	1.003	63.0
1.250	4.000	42.0	6.857	0.309	0.371	0.832	0.296	0.958	0.799	2.8393	1.012	59.4
1.300	3.333	36.4	7.912	0.305	0.366	0.833	0.292	0.957	0.798	1.9965	1.011	56.2
1.350	2.857	32.4	8.889	0.301	0.362	0.831	0.288	0.957	0.796	1.2506	1.015	53.3
1.380	2.632	30.5	9.441	0.299	0.359	0.833	0.286	0.956	0.796	0.7417	1.016	53.1
1.400	2.500	29.4	9.796	0.298	0.358	0.832	0.285	0.956	0.796			52.9

[a]Capped at 130 km in model used

[b]Best fit to ARDC model

preclude the direct application of their results to any atmospheric model. In addition, they only investigated perturbations in celerity, and did not address the question of the physical nature of potential energy (elastic vs. gravitational), which controls whether or not the wave can be considered a "tsunami". Even Tsai et al. (2013) who used a Lagrangian variational approach in their derivations, did not elaborate on E_E, and largely regarded it as negligible.

By contrast, and with an eye to applying this concept to the case of the atmosphere, we consider here a 4-km ocean featuring a large density contrast, namely $\alpha_W = 1/2$. In order to preserve the total mass of the ocean, we use $\rho_t = 750$ and $\rho_b = 1500$ kg/m³, with layer thicknesses $d_t = 2.67$ and $d_b = 1.33$ km, respectively ($\beta_W = 2/3$). These values yield $p_+ = 0.934$; note that Watada's (2013) Eq. (37) should not be used, since it assumes α_W close to 1.

Figure 10 shows the dispersion of the tsunami mode of this two-layer model, computed in the normal mode formalism, taking into account the finite compressibility of the ocean ($\alpha = 1.5$ km/s). The thin black line is the dispersion C_{one} for a one-layer ocean of constant density, and the thick red one (C_{two}) for the two-layer ocean. We note the excellent agreement

with Watada's (2013) results, shown as the blue dotted line, once the correction $p_+ = 0.934$ has been applied to C_{one}. The green dashed line shows the undispersed $C_{SWA} = 198$ m/s corrected by p_+.

The physical interpretation of p_+ is of course that because of the stratification, the mass of water is on average at a lower altitude from the bottom than in the homogeneous case, and an "effective" thickness H_{eff} should be smaller than $H_{Oc.}$, with the tsunami celerity $\sqrt{g H_{eff}}$ similarly reduced. This remark suggests characterizing H_{eff} using the altitude z_{CM} of the center of mass of the two-layer model. This is easily computed as

$$
z_{CM} = \frac{\int_0^{H_{Oc.}} \rho\, z \cdot dz}{\int_0^{H_{Oc.}} \rho \cdot dz}
= \frac{H_{Oc.}}{2} \cdot \frac{(1-\beta_W)^2 + \alpha_W\left[1-(1-\beta_W)^2\right]}{1-\beta_W + \alpha_W \beta_W}. \tag{7}
$$

With the above values for the parameters of the two layers, an intuitive estimate would be $H_{eff} = 2 z_{CM} = (5/6) H_{Oc.}$, which in turn leads to a reduction in celerity by a factor $p_{CM} = \sqrt{H_{eff}/H_{Oc.}} = 0.913$. It is shown applied to C_{one} as the brown dotted line on Fig. 10. While it overcorrects with respect to the

exact p_+, it remains an acceptable estimate of the effect of layering. More generally, on Fig. 11 we compare contours of the functions p_+, obtained as the square root of (6), and p_{CM} obtained from the estimate (7) of the center of mass of the column. While the two corrections differ somewhat for very large β_W and very small α_W, they remain within 10% of each other over 80% of the plot. This further suggests using twice the altitude of the center of mass for H_{eff} to obtain an estimate of celerity in the case of a strongly compressed fluid.

Turning our attention to the effect of layering on the elastic fraction of potential energy, we plot in Fig. 12 the ratio E_E/E_P as a function of frequency for the two-layer (solid line) and one-layer (dashed line) 4-km oceans. We find that layering has a minimal effect, even at the shortest periods considered here, for which the ratio decreases by an amount of only 0.74% to 0.68%. Note that our results for the one-layer case differ slightly from Okal's (1982) who considered an ocean with a rigid bottom (his Table 1, p. 5). In our model, the wave penetrates, albeit weakly, the solid Earth where its energy is mostly elastic, thus increasing the ratio at a period of 1000 s by 0.86%, as opposed to 0.57% in Okal's (1982) model, but these numbers remain in any case very small. We conclude that layering does not affect the physical nature of the wave, which remains a gravitational oscillation, and therefore a genuine tsunami.

In conclusion of this section, we have expanded the work of Okal (1982) for the tsunami of a liquid oceanic column. We confirm that, as the compressibility of seawater is increased (α decreased), the potential energy of the tsunami becomes increasingly elastic, over the entire range of frequencies considered. When the speed of sound α becomes comparable to, or smaller than $\sqrt{g\,H_{Oc.}}$, the wave loses its nature as a gravitational oscillation, and thus ceases to be a tsunami.

4. Atmospheric α Close to C: Not a Coincidence

In Sect. 2, we have established that the mode GR_0 cannot be regarded as the "tsunami" of the atmospheric column since it represents an oscillation between kinetic energy and overwhelmingly elastic potential energy, and the structure of its eigenfunction in the troposphere deviates fundamentally from that of a tsunami (Fig. 3). Section 3 has hinted that this effect is rooted in the similarity between the celerity C of GR_0 (taken as its undispersed value at low frequencies, ~ 315 m/s) and the speed of sound, at least in the dense layers of the lower atmosphere ($\alpha = 340$ m/s).

We show here that this similarity is not coincidental, but rather expected if the atmosphere is modeled as a perfect gas. We first recall that the speed of sound α of a gas (in particular of the atmosphere) was first given as $\sqrt{P/\rho}$ by Newton (1687), building on the results of Boyle (1662). It was later corrected to $\sqrt{\gamma P/\rho}$ by Laplace (1805) who recognized the adiabatic rather than isothermal nature of the vibration. In modern notation, α is given at each altitude z by

$$\alpha = (K_S/\rho)^{1/2} = (\gamma P/\rho)^{1/2} = (\gamma R \Theta/M)^{1/2} \quad (8)$$

where Θ is the absolute temperature at altitude z, $R = 8.32$ J·kg^{-1}·mole^{-1} the molar gas constant, and $M \approx 0.029$ kg/mole the molar mass of air. γ is the familiar ratio of heat capacities at constant pressure and volume, which takes the value 1.4 for a diatomic gas. In the real atmosphere, and despite its great rarefaction with height, Θ and hence α vary only slightly through the atmospheric column (Fig. 1).

A fundamental argument is then that the pressure P in (8) follows $dP = -\rho\,g\,dz$, and thus can be expected, in the lower, dense layers of the atmosphere to take the form

$$P = \rho_0\,g\,\cdot\,H_P \quad\quad (9)$$

where H_P is an "effective" thickness of the atmosphere.

Meanwhile, under the SWA, the celerity of a tsunami is expected to be

$$C = (g\,\cdot\,H_{eff})^{1/2} \quad\quad (10)$$

where H_{eff} is another appropriate "effective thickness" of the atmosphere, which, as argued in Sect. 3, might be approximated by $2\,z_{CM}$ where z_{CM} is the altitude of the center of mass of the horizontal layering of the atmosphere.

Then, the ratio of the velocities α and C takes the simple form

$$\frac{\alpha}{C} = \left(\gamma H_P / H_{eff}\right)^{1/2}. \tag{11}$$

There is no reason why the two thicknesses H_P and H_{eff} should be equal, but since they represent different averages of the properties of an atmospheric layering, they would be expected to be of a *comparable order of magnitude*, which in turn would make the ratio (11) close to 1, and according to the results of Sect. 3, rule out the development of a "tsunami", i.e., a gravitational oscillation, in the atmosphere.

In this section, we consider a number of theoretical models of atmospheric layering, and compare the theoretical values of C and α with their numerical counterparts. Specifically, we discuss them in the context of L10, whose work forms the basis of several later developments. Here, we summarize his results on the propagation of fundamental atmospheric oscillations, with many details regrouped in Appendix 2, notably regarding his notation.

In very general terms, L10 first considers two limiting models of the atmosphere, an isothermal one in which $P/\rho = $ cnst, and an isentropic one, where $P/(\rho^\gamma) = $ cnst. The first model had been used by Laplace (1805), and L10 points out that author's use of a purely horizontal particle motion, an assumption which we would regard as plausible, given the results of Sect. 2. L10 (p. 553) then argues that such a "longitudinal wave" would be close to an acoustic signal propagating horizontally as a sound wave at the "Newtonian" velocity of sound $C = \sqrt{R\Theta/M}$, apparently neglecting the adiabatic correction $\sqrt{\gamma}$ introduced by Laplace. L10 then defines

$$H = \frac{R\Theta}{Mg} \tag{12}$$

which immediately gives C the form $\sqrt{gH}$, suggesting that the wave is indeed the gravitational oscillation of a fluid layer of thickness H, albeit without any physical justification regarding its structure. Note in particular that this interpretation would contradict L10's previous assertion that the wave is "close to an acoustic signal". H can be interpreted as the thickness of a homogeneous

atmosphere ($\rho = \rho_0 = $ cnst) whose weight creates the pressure P_0 observed at the Earth's surface.

The isothermal and isentropic layerings can be regarded as end members of a continuum of models featuring

$$P/(\rho^\phi) = \text{cnst}, \tag{13}$$

with $\phi = 1$ and $\phi = \gamma = 1.4$, respectively.

• For all $\phi \neq 1$, these models are characterized by a linear variation of Θ with height:

$$\Theta = \Theta_0 \cdot \left[1 - \frac{\phi - 1}{\phi} \frac{gM}{R\Theta_0} \cdot z\right] \tag{14}$$

and fractional power law variations of P and ρ:

$$\begin{aligned} P &= P_0 \cdot \left[1 - \frac{\phi - 1}{\phi} \frac{gM}{R\Theta_0} \cdot z\right]^{m\phi} \\ \rho &= \rho_0 \cdot \left[1 - \frac{\phi - 1}{\phi} \frac{gM}{R\Theta_0} \cdot z\right]^{m} \end{aligned} \tag{15}$$

where $m = 1/(\phi - 1)$ in the notation of L10 (see Appendix 2). Equation (14) leads to absolute zero temperature ($\Theta = 0$) at an altitude

$$\zeta = \frac{\phi}{\phi - 1} \cdot \frac{R\Theta_0}{gM} = m\phi \cdot H. \tag{16}$$

Since Θ cannot be negative, the atmosphere then has the finite height ζ.

• For $\phi = 1$ (isothermal layering), the pressure and density of the atmosphere vary as $\exp(-z/H_\Theta)$, with $H_\Theta = R\Theta/Mg$, and the "height" ζ of the atmosphere becomes infinite. Note that H_Θ is equivalent to L10's H introduced above (12).

• For $\phi < 1$, the temperature would increase regularly with height, which clearly does not apply to the troposphere and stratosphere, although it could apply locally in the upper layers of the atmosphere (e.g., above 100 km).

• For $\phi > 1$, Eq. (14) holds, and the atmosphere has the finite thickness ζ. That underscores the unrealistic application of such models to the full atmosphere, which can however approach such conditions over a *finite* range of altitudes. We note in particular that the temperature Θ in the portion of the ARDC model in which it decreases with height ($z < 95$ km) is best-fit with a parameter $\phi = 1.032$, before Θ starts rising fast at greater heights.

• The isentropic model is reached for $\phi = \gamma = 1.4$, the thickness of the atmosphere being $\zeta_S \approx 29.4$ km $= (7/2)H$ in L10's notation (see Appendix 2), and the gradient $\Theta_0/\zeta_S = 9.8$ K/km being known as the "lapse rate" in atmospheric physics (e.g., Kittel & Kroemer, 1980, p. 179).

•, For $\phi > \gamma = 1.4$ (superadiabatic layering), the atmosphere is unstable and convects.

Thus, legitimate values of ϕ in (13–16) are in the interval $[1, \gamma]$. L10 then generalizes his study to all such values, parameterizing the models through the temperature gradient β, which ranges from 0 to the lapse rate (β_1 in his notation, for which we prefer β_S for "isentropic"):

$$\beta_S = \beta_1 = \frac{2}{7} \frac{\Theta_0}{H}. \quad (17)$$

There follows in L10 a rather arcane mathematical derivation of the dispersion of the "Lamb wave" (which corresponds to Harkrider's 1964 GR_0 branch) through the roots of his Equation (63, p. 563):

$$\frac{1}{2} \xi J_{m+1}(\xi) = \left[\frac{\beta_S}{\beta} - 1\right] J_m(\xi) \quad (18)$$

where J_v is the regular Bessel function of order v, and $m = 1/(\phi - 1)$. Equation (18) assumes a low-frequency limit (wavelength much larger than the various scales of the atmosphere); the solution for the celerity C of the Lamb wave GR_0 is then found through L10's Equation (66, p. 563):

$$C^2 = \left[\frac{\beta_S}{\beta} - 1\right] \cdot \frac{4(m+1)gH}{\xi^2} \quad (19)$$

where ξ is the first non-zero root of (18). Solutions for undertones such as the Pekeris mode GR_2 would use subsequent roots of (18) as ξ in (19). Unfortunately, these results do not lend themselves to easy numerical computation, with quantities such as the bracket in (18) varying from 0 (isentropic) to infinity (isothermal). In practice, values of ξ can be easily estimated only when they are large or small compared to 1, or when m is an integer plus 1/2, in which case L10 was able to manually compute J_m using trigonometric functions.

In the following sub-sections, we follow L10's approach and consider a full range of various atmospheric models of the type (13) with $(1 \leq \phi \leq 1.4)$. We use the center-of-mass model to obtain estimates of the celerity C_ϕ of a would-be tsunami as a function of ϕ, and most importantly of the ratio α/C_ϕ, which Sect. 3 has suggested controls whether or not the resulting Lamb wave can be considered a "tsunami" of the atmosphere. Most of these models are of course at least locally inappropriate, but arguably they can provide a range of possible structures approaching the conditions of the real atmosphere, and as such give physical insight into the problem. We will find that for $1 \leq \phi \leq 1.4$, the ratio α/C_ϕ remains remarkably constant at ~ 0.83.

4.1. The Isothermal Model ($\phi = 1$ or $\beta = 0$ in L10's Notation)

As mentioned earlier, the concept was used originally by Newton (1687) and later Laplace (1805). An isothermal structure was also used e.g., by Kanamori et al. (1994) to model the waves of the 1991 Pinatubo explosion. It would be expected to be a fair representation of the ARDC model, since the latter can be regressed with $\phi = 1.032$ in its part featuring substantial material density ($z < 95$ km).

* Speed of sound α

In an isothermal atmosphere, α will be constant, and equal to

$$\alpha_\Theta = (\gamma R \Theta/M)^{1/2} = (\gamma gH)^{1/2} = 340 \text{ m/s} \quad (20)$$

for $\Theta = 288$ K, the average temperature at the Earth's surface.

* Celerity C of a would-be tsunami

In this case, the density ρ varies with height z as

$$\rho(z) = \rho_0 \exp(-z/H) \quad (21)$$

with $H = R\Theta/Mg \approx 8.4$ km, as defined by L10 [see (12) above]. Following Sect. 3, we estimate H_{eff} as twice the altitude z_{CM} of the center of mass of the atmospheric column, $[z_{CM} = \int_0^\infty z \rho(z) \cdot dz / \int_0^\infty \rho(z) \cdot dz = H]$, so that $H_{eff} = 2H$. The celerity of a would-be tsunami under the SWA will be

$$C_\Theta = \sqrt{2gH} \approx 408 \text{ m/s} \quad (22)$$

for $\Theta = 288$ K.

4.2. The General Case $\phi \neq 1$

In this model, the atmospheric layering satisfies $P/(\rho^{\phi}) = $ cnst, with ϕ strictly greater than 1 (and not greater than $\gamma = 1.4$); the atmosphere has the finite thickness $\zeta = m\phi H$ (16).

* Would-be tsunami velocity

To obtain an estimate of H_{eff} we compute the altitude of the center of mass of the column

$$z_{CM} = \frac{H_{eff}}{2} = \frac{\int_0^{\zeta} z\,\rho(z)\cdot dz}{\int_0^{\zeta} \rho(z)\cdot dz} \tag{23}$$
$$= \frac{\zeta}{m+2} = \frac{\phi}{2\phi-1}\cdot H.$$

Hence, the undispersed SWA celerity of the would-be tsunami is estimated at

$$C_{\phi} = \left[\frac{2\phi}{2\phi-1}\;gH\right]^{1/2}. \tag{24}$$

* Speed of sound

In order to obtain an estimate of the average speed of sound, we consider the average of $\sqrt{\Theta}$, weighted by the density at each altitude z

$$\langle\sqrt{\Theta}\rangle = \frac{\int_0^{\zeta} \rho\,\sqrt{\Theta}\cdot dz}{\int_0^{\zeta} \rho\cdot dz}$$
$$= \sqrt{\Theta_0}\,\frac{\int_0^{\zeta}(1-z/\zeta)^{1/2}\,(1-z/\zeta)^m\cdot dz}{\int_0^{\zeta}(1-z/\zeta)^m\cdot dz} \tag{25}$$
$$= \sqrt{\Theta_0}\cdot\frac{m+1}{m+3/2}.$$

Hence

$$\alpha_{\phi} = \sqrt{\gamma R/M}\,\langle\sqrt{\Theta}\rangle = \frac{2\,\phi}{3\phi-1}\cdot\sqrt{\gamma\,gH}. \tag{26}$$

Another estimate can be obtained by averaging Θ rather than $\sqrt{\Theta}$. Equation (25) is replaced by

$$\langle\Theta\rangle = \frac{\int_0^{\zeta} \rho\,\Theta\cdot dz}{\int_0^{\zeta}\rho\cdot dz} = \Theta_0\,\frac{\int_0^{\zeta}(1-z/\zeta)^{m+1}\cdot dz}{\int_0^{\zeta}(1-z/\zeta)^m\cdot dz}$$
$$= \Theta_0\,\frac{m+1}{m+2} = \frac{\phi}{2\phi-1}\,\Theta_0$$
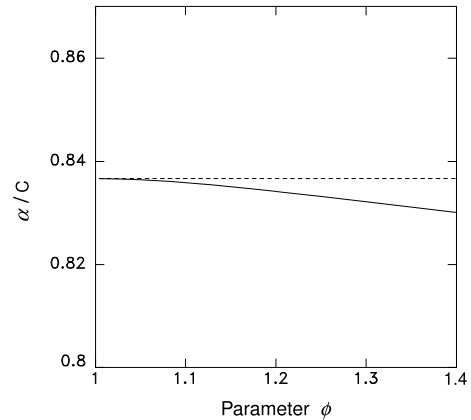$$\tag{27}$$

and then (26) by:

Figure 13
The solid line plots the ratio α_{ϕ}/C_{ϕ} (33) of average sound velocity (26) to celerity of the GR_0 mode computed from the center of mass approximation (24), as a function of the parameter ϕ. The dashed line uses α'_{ϕ} (28) instead

$$\alpha'_{\phi} = \sqrt{\gamma R\langle\Theta\rangle/M} = \sqrt{\frac{\phi}{2\phi-1}}\cdot\sqrt{\gamma\,gH}. \tag{28}$$

4.3. The Special Case of the Adiabatic (Isentropic) Model ($\phi = \gamma$ or $\beta = \beta_1$)

As a limiting case of the above models, the isentropic layering has received particular attention, notably from L10. The Brunt–Väisälä frequency (1) then vanishes, and there is no gravitational restoring force to an adiabatic vertical displacement of a particle of atmosphere. However, a heterogeneous horizontal displacement entices a local change of volume and hence of density, which does contribute a change in potential and hence a gravitational component to the restoring force.[3]

In this particular case, the celerity C_S computed from (24) is 358 m/s for $\Theta_0 = 288$ K at the bottom of the atmosphere, the average sound velocity (26) is $\alpha_S = (7/8)\sqrt{\gamma gH} = 297$ m/s and the alternative estimate (28) is $\alpha'_S = 300$ m/s, those two values differing by only 1%.

---

[3] A physical explanation of this situation is that the "free air" component of the restoring force (due to displacement in a gravity field including buoyancy) vanishes, but the "Bouguer" one (due to a change in that field upon a change of material properties) does not.

We note that the dispersion of the tsunami of an adiabatically stratified ocean column was investigated by Tsai et al. (2013) and Watada (2013) who obtained, as a counterpart to p_+ defined in (6), a correction

$$p_{Adiab} = 1 - \frac{\rho_b - \rho_t}{4\,\rho_{avg.}}. \tag{29}$$

However, their approach assumed a small correction, i.e., p_{Adiab} close to 1, which does not hold if applied to the present atmospheric model ($\rho_t = 0$; $\rho_b = \rho_0$; $\rho_{avg.} = \rho_0/(m+1) = (2/7)\rho_0$), yielding $p_{Adiab} = 1/8$ and $C_{Adiab} = 45$ m/s, which renders the method inapplicable. This is due to their tacit assumption of a weak stratification, or ($\rho_b - \rho_t \ll \rho_{avg.}$), clearly violated by the atmospheric model considered here.

The theoretical values of all parameters $(m, \zeta, \beta, \alpha_\phi, C_\phi)$ are compiled as a function of ϕ in the left part of Table 1 (first seven columns).

4.4. The ARDC Model

Finally, we consider the ARDC model and compute the average value of α as

$$\alpha_{ARDC} = \frac{\int_0^{z_{top}} \alpha(z)\,\rho(z)\,\cdot\,dz}{\int_0^{z_{top}} \rho(z)\,\cdot\,dz} = 317 \text{ m/s} \tag{30}$$

between the Earth's surface and $z_{top} = 130$ km, and the expected celerity of a would-be tsunami under the SWA in the center of mass model

$$C_{ARDC} = \sqrt{2\,g\,z_{CM}} = 380 \text{ m/s} \quad \text{with}$$
$$z_{CM} = \frac{\int_0^{z_{top}} z\,\rho(z)\,\cdot\,dz}{\int_0^{z_{top}} \rho(z)\,\cdot\,dz} = 7.2 \text{ km}. \tag{31}$$

5. Discussion and Conclusion

5.1. General Discussion

• For $\phi = 1$ (isothermal model), the combination of Eqs. (20) and (22) leads to a ratio

$$\frac{\alpha_\Theta}{C_\Theta} = \sqrt{\gamma/2} \approx 0.837. \tag{32}$$

• For other values of ϕ, and combining (24) and (26)

$$\frac{\alpha_\phi}{C_\phi} = \frac{2\phi\,\sqrt{\gamma}}{3\phi - 1} \cdot \sqrt{1 - 1/2\phi} \tag{33}$$

or, using the alternative estimate of sound velocity (27)

$$\frac{\alpha'_\phi}{C_\phi} = \sqrt{\gamma/2} \approx 0.837 \tag{34}$$

this last result being, remarkably, independent of ϕ and exactly equal to (32). As illustrated on Fig. 13, even the ratio (33) varies only very slightly, from the value (32) for $\phi = 1$ to $[2\gamma/(3\gamma - 1) \cdot \sqrt{\gamma - 1/2}] \approx 0.830$ for $\phi = \gamma = 1.4$. In addition, the ratio (33) is continuous with (32) as $\phi \to 1$, even though (24) and (26) did not strictly apply for $\phi = 1$.

• As for the ARDC model, the ratio of the estimates (30) and (31) is also found to be

$$\frac{\alpha_{ARDC}}{C_{ARDC}} = 0.835 \tag{35}$$

in excellent agreement with the ratios $\alpha_{1.032}/C_{1.032} = 0.8366$ and $\alpha'_{1.032}/C_{1.032} = 0.8367$ obtained by setting the regressed slope $\phi = 1.032$ in Eqs. (33) and (34). However, we note that the use of the center of mass model for C_{ARDC} overestimates its observed value (313 m/s) or that computed in Sect. 2 (312 m/s).

These results indicate that for all legitimate values of ϕ, we predict a sound velocity comparable to, but lower than, the would-be tsunami velocity, estimated as $\sqrt{2\,g\,z_{CM}}$. Consequently, the results of Sect. 3 suggest strong coupling between the elastic and gravitational components of the restoring force, and therefore predict that no tsunami can develop inside any of the layered structures considered.

While in all cases, the velocities C are found slightly greater than α, the important result is that they are fundamentally *on the same order of magnitude*. The robustness of the ratios (32–35) for significantly different models of atmosphere suggests that this general equivalence of α and C is an intrinsic property of the atmosphere as a perfect gas, rather than a fortuitous occurrence. We recall that, by contrast, the same ratio for an ocean of realistic depth is always greater than 6 (for a 6-km deep ocean), and even larger in shallower seas.

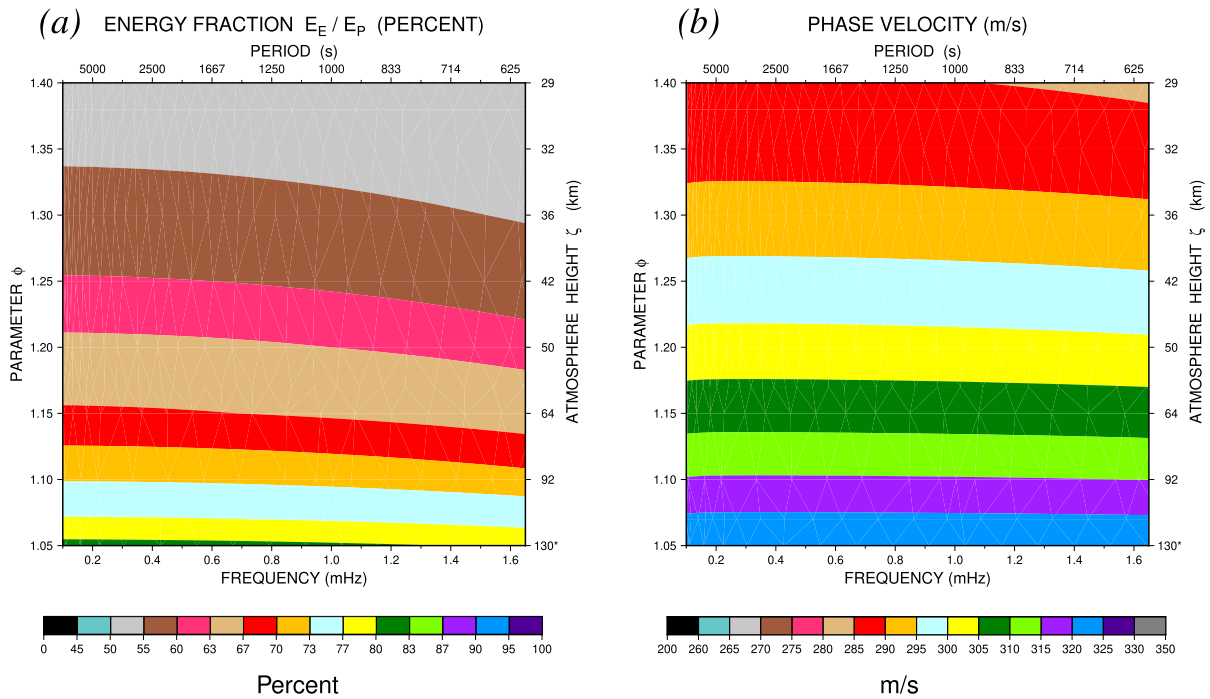We thus come to the conclusion that, contrary to a liquid whose compressibility remains moderate, a

Figure 14

a Contour plot of the ratio of elastic to total potential energy of the GR_0 modes, as a function of frequency and parameter ϕ, for various models of atmospheric layering. Note the strong dependence on ϕ, and the weaker one on frequency, especially at lower values of ϕ. However, the ratio always remains greater than 50%. **b** Same as **a** for the computed celerity C. Note its systematic decrease with increasing ϕ, and the very weak dependence on frequency except when ϕ approaches its isentropic value (1.4)

perfect gas subject to a gravity field gets stratified to an extent where the velocity of a would-be tsunami will necessarily be comparable to α, and the potential energy of the wave primarily elastic.

In short, a perfect gas such as the atmosphere cannot sustain a tsunami, defined as an oscillation between kinetic and gravitational energy.

5.2. Comparison with Numerical Values of the Celerity of GR_0

We then compare these theoretical estimates of would-be tsunami celerities to actual values along the GR_0 branch obtained by running our normal mode algorithm on models of atmospheric layering of the form (13) with ϕ varying between 1.0 and 1.4. We keep the temperature constant at the bottom of the atmosphere ($\Theta_0 = 288$ K). For $\phi \leq 1.05$, the model is capped at an altitude of 130 km, otherwise at the altitude ζ given by (16). For each model, we compute

the GR_0 eigenfunction, and in particular its celerity C, taken along the undispersed part of the branch, and the elastic portion of the potential energy, E_E/E_P, in the frequency range 0.1–1.67 mHz ($T = 600$–10000 s). We compile their values in the right part of Table 1 (last six columns), as well as the ratios C/α_ϕ and C/C_ϕ. Finally, we recompute the parameter ζ defined in (18) by using the actual phase velocity C of the GR_0 wave to recast (19) into

$$\xi^2 = (\beta_S/\beta - 1) \cdot \frac{4\,(m+1)\,gH}{C^2} \qquad (36)$$

and we form the ratio

$$TEST = \frac{\xi}{2} \cdot \frac{\beta}{\beta_S - \beta} \cdot \frac{J_{m+1}(\xi)}{J_m(\xi)} \qquad (37)$$

which characterizes the fit of the actual celerity C to a root of the Bessel equation (18). We find that this fit is excellent ($TEST = 1$ within 2%), even when approaching the end-member values $\phi \to 1$ or 1.4. This constitutes an independent verification of the

Figure 15
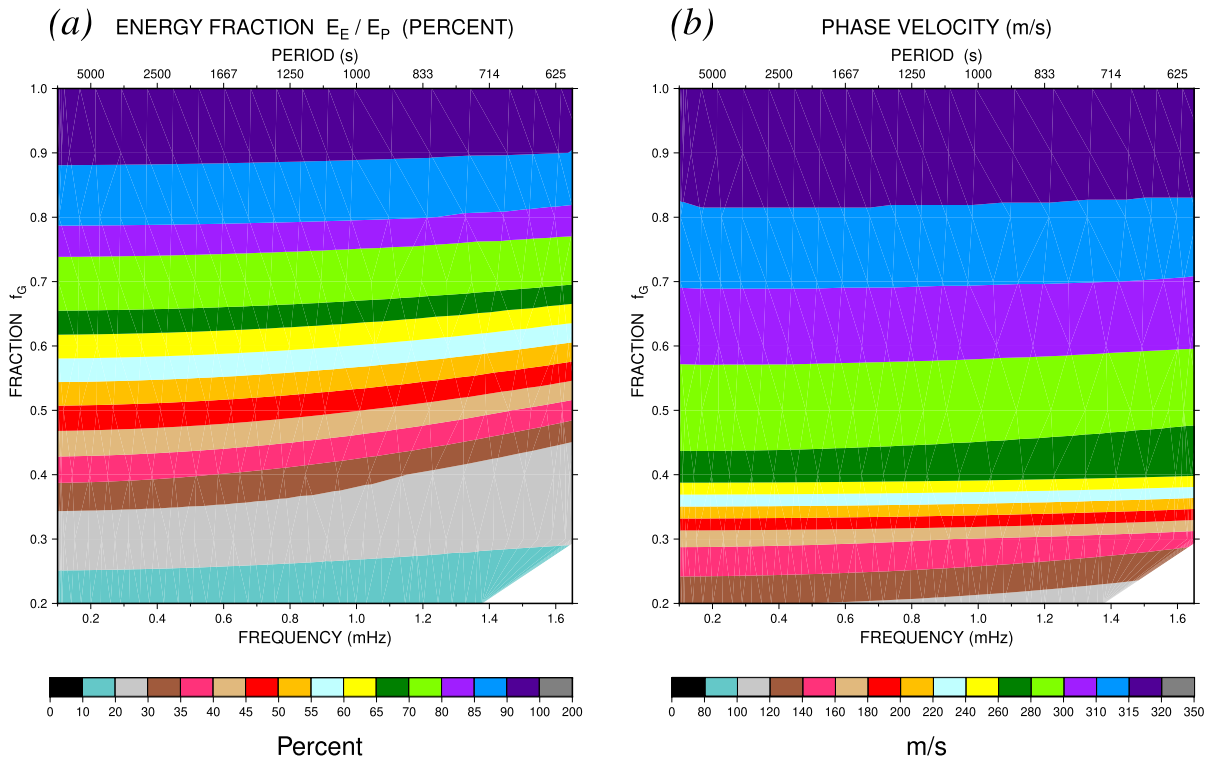
Energy fraction (**a**) and phase velocity (**b**) of the GR_0 branch contoured as a function of frequency and of the fraction f_G by which the restoring gravity force is artificially reduced in the experiment of Sect. 5.3. Note that for very low values of f_G, the energy becomes predominantly gravitational, which would qualify the wave as a tsunami. By then, the atmosphere has, arguably, become a "liquid"

dispersion of Lamb waves, and in particular of the approximations underlying the derivation of L10's Equations (63) and (66), p. 563.

We also find that the ratio C/α_ϕ remains between 0.95 and 1 for all values of ϕ, which brings support to the general concept of the Lamb wave being of an elastic nature, traveling at close to a *sound velocity*, appropriately averaged over the atmospheric structure.

By contrast, we see in Column 10 of Table 1 that C is always deficient with respect to the celerity C_ϕ expected for a would-be tsunami (modeled under the center-of-mass approximation), and increasingly so as ϕ grows from 1 to 1.4. This simply confirms, if need be, that the GR_0 wave *cannot* be regarded as a tsunami of the atmosphere for which the celerity C should match the estimate C_ϕ.

In addition, Fig. 14a contours the elastic fraction of the potential energy, E_E/E_P; it exhibits a strong dependence on ϕ and a weaker one on frequency, but remains greater than 50% over the full domain of study, again confirming that the GR_0 branch does *not* constitute a gravitational oscillation.

5.3. A Final, Perhaps Outrageous but Insightful, Experiment

In this context, it is worth re-examining Harkrider and Press' (1967, p. 153) statement that "when gravity is reduced to zero, [...] the GR waves vanish". Indeed, we have verified that the GR branches disappear in the total absence of gravity, which reduces from 6 to 4 the dimension of the eigenvector y_i in Saito's (1967) formalism (Appendix 1).

Here, we further explore this question by keeping the 6-dimensional problem, but artificially reducing the gravity field g (and the gravitational constant G) by a factor f_G in all steps of the calculation, *while maintaining the material properties of the medium* (density and elastic constants). This amounts to reducing the contribution of gravity to the restoring force during the deformation, while keeping the elastic one unchanged. We do find solutions which share the characteristics of the unperturbed branch GR_0, notably its very weak dispersion. Figure 15a is a counterpart to Fig. 9, contouring the ratio E_E/E_P between 0.1 and 1.65 mHz (10000 to 606 s) and for f_G varying from 0.2 to 1, in the case of an oceanless ARDC structure.

The main result of this experiment is that E_E/E_P decreases when gravity is reduced, first slowly (to about 60% for $f_G = 0.6$), then rapidly, reaching values of $\sim 15\%$ for $f_G = 0.25$ (the ratio also features a minor decrease with increasing frequency, especially in the range $f_G \approx 0.4$). Under such conditions, the energy in GR_0 becomes prominently gravitational and the branch would qualify as a tsunami of the atmosphere. Figure 15b similarly contours the phase velocity of the branch GR_0; it is essentially independent of frequency, but decreases sharply at lower f_G, to velocities of ~ 130 m/s for $f_G = 0.2$, which then fit the SWA tsunami celerities for an 8.5-km fluid column, but fall to less than 40% of the [unchanged] sound velocity α.

Finally, we have verified that, for $f_G = 0.2$ and a period $T = 1000$ s ($l = 357$), the ellipticity of particle motion ($l\, y_3/y_1$) at an altitude of 10 km takes a value of 2.09, in good agreement with that predicted (2.23) by Eq. (3) under the SWA for $g = 1.96$ m/s^2 (as opposed to about 30 times larger in the real atmosphere).

In short, all this evidence qualifies the GR_0 wave simulated under these conditions as a genuine tsunami, which would seem to *negate* our previous conclusion, a result especially troubling since it occurs *for the lowest values of f_G*.

The origin of this paradox lies in our assumption of unperturbed mechanical properties (density, sound velocity). As a result, we have created an artificial medium no longer behaving as a perfect gas, and in particular featuring a bulk modulus K_S much larger

than the ambient pressure at equilibrium, controlled by the integral of $dP = -\rho g\, dz$. Such properties are more characteristic of a *liquid* than of a gas, and consequently, our medium may indeed become a "virtual liquid", able to sustain a tsunami.

While the model considered in this sub-section has of course no application to the real Earth, we believe that it brings insight into the fundamental question of what distinguishes a liquid from a [perfect] gas. As a form of condensed matter, the former has intrinsic mechanical properties (ρ, K) largely insensitive to pressure and hence to gravity; in simple terms, a liquid is highly incompressible. For example, at the bottom of a 5-km deep ocean, the pressure is 50 MPa, 500 times that at the surface, but remains 45 times less than the water's bulk modulus (2.3 GPa). As a result, the density of seawater has increased by only $\sim 2\%$ and the speed of sound by no more than 6% (UNESCO, 1981). By contrast, in a gas, K_Θ is identical to P, and K_S follows suit. In the virtual medium we have considered, and for $f_G = 0.2$, we have increased the K_S/P ratio by a factor of 5 with respect to the actual atmosphere, which is enough to disqualify it as a "gas". In the presence of reduced gravity, a true gas would feature a much weaker stratification and lower values of P, and hence K_S, leading to strong coupling and a kind of consanguinity between elastic and gravitational properties.

The bottom line of this experiment, and the conclusion of this paper, is that the mere presence of gravity, however small (but finite) it may be, will segregate the mechanical and hence elastic behavior of liquids and gases, and prevent the latter from sustaining tsunamis.

Appendix 1

We recall here the definition of the 6 components of the eigenvector of a spheroidal mode in the formalism of Saito (1967, p. 3690), later used by Kanamori and Cipar (1974).

• $y_1(r)$ represents the vertical (radial) component of particle motion, given as

$$u_r(r, \theta, \phi; t) = y_1(r) Y_l^m(\theta, \phi). \qquad (38)$$

• $y_2(r)$ represents the radial component of the traction, given as

$$\sigma_{rr}(r, \theta, \phi; t) = y_2(r) Y_l^m(\theta, \phi). \qquad (39)$$

• $y_3(r)$ represents the orthoradial component of particle motion, given as

$$u_\theta(r, \theta, \phi; t) = y_3(r) \frac{\partial Y_l^m(\theta, \phi)}{\partial \theta}. \qquad (40)$$

• $y_4(r)$ represents the shear component of the traction, given as

$$\sigma_{r\theta}(r, \theta, \phi; t) = y_4(r) \frac{\partial Y_l^m(\theta, \phi)}{\partial \theta}. \qquad (41)$$

• $y_5(r)$ represents the change in gravity potential, given as

$$\psi(r, \theta, \phi; t) = y_5(r) Y_l^m(\theta, \phi). \qquad (42)$$

• Finally, $y_6(r)$ is simply defined as

$$y_6(r) = \frac{dy_5(r)}{dr} - 4\pi G \rho y_1(r) \qquad (43)$$

where the Y_l^m are the spherical harmonics of degree l and order m. In all above equations, the time dependence $e^{i\omega t}$ has been omitted for simplicity.

Obviously, y_1 and y_3 have dimensions of length, y_2 and y_4 of pressure, y_5 of velocity squared, and y_6 of acceleration.

In this fashion, all boundary conditions between spherical shells with different mechanical properties simply require the continuity of the six components of the vector **y**, with the exception of y_3 when at least one of the layers is fluid.

Note that in all fluid layers (outer core, ocean, atmosphere), y_4 is identically zero, and y_3 becomes a spurious variable

$$y_3 = \frac{1}{r \omega^2} \left[g y_1 - \frac{y_2}{\rho} - y_5 \right] \qquad (44)$$

so that the differential system becomes 4-dimensional. Also, in a fluid, y_2 is simply the opposite of the overpressure during the oscillation.

Finally, for large l and θ not close to 0 or π, asymptotic expansions of the Y_l^m show that the partial derivative in (40) results in an orthoradial particle displacement u_θ of order $(l y_3)$ while the vertical component remains of order y_1.

Appendix 2

We summarize here some of the steps in L10's derivation of his Equations (63) and (66) p. 563. In particular, we emphasize the occasionally different notation used in his paper.

1. Note that L10 orients the vertical axis (which he calls y) downwards with the origin at the top of the atmosphere, which is infinite in the isothermal model and otherwise depends on the particular structure used. On the other hand, we call it z and orient it upwards, with the origin consistently at the bottom of the atmosphere.

2. For a layering of the form (13), L10 does not use the parameter ϕ, but rather defines the [absolute] temperature gradient

$$\begin{aligned} \beta &= -\frac{d\Theta}{dz} = \frac{\phi - 1}{\phi} \cdot \frac{\Theta_0}{H} \\ &= \frac{\phi - 1}{\phi} \cdot \frac{gM}{R} \quad \text{(units: K/km)}. \end{aligned} \qquad (45)$$

Conversely,

$$\phi = \frac{1}{(1 - \beta R/Mg)} = \frac{1}{(1 - \beta H/\Theta_0)} \qquad (46)$$

with H defined as

$$H = \frac{R\,\Theta_0}{M\,g} \qquad (12)$$

(Note that L10's notation is R for our R/M).

3. Define

$$m = \frac{1}{\phi - 1} = \frac{\Theta_0}{\beta H} - 1 = \frac{gM}{R\beta} - 1 \quad \text{(dimensionless)}. \qquad (47)$$

Note that Lamb's notation is n in L10; m in Lamb (1932).

4. Define h as the full height of the atmosphere

$$h = \frac{\Theta_0}{\beta} = \frac{\phi}{\phi - 1} \cdot H = m\,\phi\,H \qquad (48)$$

where h is defined in Eq. (12). h is equivalent to our ζ in (16).

5. For the isentropic case ($\phi = \gamma = 1.4$)

$$\beta = \beta_S = \frac{2}{7} \cdot \frac{\Theta_0}{H} \quad m = m_S = \frac{5}{2} \quad h = h_S = \frac{7}{2}\,H. \qquad (49)$$

(L10's notation: $\beta_S = \beta_1$).

6. For the isothermal case ($\phi = 1$)

$$\beta = \beta_\Theta = 0$$
$$m = m_\Theta \;\rightarrow\; \infty \quad h = h_\Theta \;\rightarrow\; \infty. \qquad (50)$$

7. Note that L10 uses V for the celerity of the atmospheric "Lamb" wave (our C), and c for the speed of sound (our α).

8. In the course of his derivation, L10 uses the potentially confusing notation $\Pi(x)$ for the factorial: $\Pi(x) = \Gamma(x+1)$ (x real) or $x!$ (x integer), even though the latter had been introduced one century earlier by Kramp (1808).

9. Then, after considerable algebra, L10 derives the solution of the dispersion through the roots of his Equation (63 p. 563) reproduced here as (18), the celerity C of the Lamb wave being given by his Equation (66), reproduced as (19).

In (18) and (19), we prefer the notation ξ, instead of L10's ω, that dimensionless variable having no relation to an angular frequency.

10. In the limit of large m ($\phi \to 1$), and in the long-wavelength approximation, ξ is expected to itself be large, and one can use Abramowitz and Stegun's (1965) Equation (9.3.1) p. 365:

$$J_m(z) \approx \frac{1}{\sqrt{2\pi m}} \cdot \left[\frac{e\,z}{2\,m}\right]^m. \qquad (51)$$

Hence

$$\frac{z\,J_{m+1}(z)}{2\,J_m(z)} = \frac{e\,z^2}{4} \cdot \sqrt{m/(m+1)} \cdot \frac{m^m}{(m+1)^{m+1}}$$
$$= \frac{e\,z^2}{4\,(m+1)} \cdot [m/(m+1)]^{m+1/2}. \qquad (52)$$

The solution to (17) is then

$$\xi^2 = (\beta_S/\beta - 1) \cdot \frac{4(m+1)}{e} \cdot [(m+1)/m]^{m+1/2} \qquad (53)$$

and substituting into L10's Equation (66) p. 563,

$$C^2 = gH \cdot \frac{e}{(1 + 1/m)^m} \cdot (1 + 1/m)^{-1/2}. \qquad (54)$$

In the limit $m \to \infty$, the fraction in (54) goes to 1, and so does the last term in parentheses, so that $C^2 \approx gH$, which justifies L10's claim that the celerity of the "Lamb" air wave observed during the Krakatau explosion coincides with that of a would-be tsunami for a column of height H defined by (12). But as shown in the present study, that does not imply that the structure of the wave is that of a tsunami.

However, the approximation (51), on which this result is based, is valid only for large m, i.e., when the layering is close to isothermal. If, on the opposite, ϕ approaches γ (isentropic layering; $m \to 5/2$), then the parenthesis $(\beta_S/\beta - 1) \to 0$ but ξ will remain finite, in practice close to 7, the first non-zero root of $J_{7/2}(\xi)$. The celerity of the Lamb wave will also approach 0 as

$$C^2 \approx (2/7)\,(\beta_S/\beta - 1) \cdot gH \qquad (55)$$

which is equivalent to L10's first [un-numbered] equation on Page 564, except for a typographic error

in the parenthesis which is identically zero as typeset in L10.

Publisher's Note Springer Nature remains neutral with regard to jurisdictional claims in published maps and institutional affiliations.

Springer Nature or its licensor (e.g. a society or other partner) holds exclusive rights to this article under a publishing agreement with the author(s) or other rightsholder(s); author self-archiving of the accepted manuscript version of this article is solely governed by the terms of such publishing agreement and applicable law.

References

Abdolali, A., & Kirby, J. T. (2017). Role of compressibility on tsunami propagation. *Journal of Geophysical Research Oceans, 122*, 9780–9794.

Abramowitz, M., & Stegun, I. (1965). *Handbook of mathematical functions* (8th ed.). Dover.

Ben-Menahem, A. (1975). Source parameters of the Siberian explosion of June 30, 1908 from analysis and synthesis of seismic signals at four stations. *Physics of the Earth and Planetary Interiors, 11*, 1–35.

Boyle, R. (1662). *A defence of the doctrine touching the spring and weight of the air.* Robinson.

Brunt, D. (1927). The period of simple vertical oscillations in the atmosphere. *Quarterly Journal of the Royal Meteorological Society, 53*, 30–32.

Carvajal, M., Sepúlveda, I., Gubler, A., & Garreaud, R. (2022). Worldwide signature of the 2022 Tonga volcanic tsunami. *Geophysical Research Letters, 49*, e2022GL098153.

Dahlen, F. A., & Tromp, J. (1998). *Theoretical global seismology.* Princeton University Press.

Dean, R. G., & Dalrymple, R. A. (2000). *Water wave mechanics for engineers and scientists.* World Scientific.

Donn, W. L., & Ewing, W. M. (1962). Atmospheric waves from nuclear explosions—Part II: The Soviet test of 30 October 1961. *Journal of Atmospheric Sciences, 19*, 264–273.

Dziewonski, A. M., & Anderson, D. L. (1981). Preliminary reference Earth model. *Physics of the Earth and Planetary Interiors, 25*, 297–356.

Ewing, W. M., & Press, F. (1955). Tide-gage disturbances from the great eruption of Krakatoa. *Transactions of the American Geophysical Union, 36*, 53–60.

Gill, A. E. (1982). *Atmosphere-ocean dynamics.* Academic Press.

Gusman, A. R., Roger, R., Noble, C., Wang, X., & Power, W. (2022). The 2022 Hunga Tonga-Hunga Ha'apai Volcano air-wave generated tsunami. *Pure and Applied Geophysics, 179*, 3511–3525.

Harkrider, D. G. (1964). Theoretical and observed acoustic-gravity waves from explosive sources in the atmosphere. *Journal of Geophysical Research, 69*, 2595–5321.

Harkrider, D. G., & Press, F. (1967). The Krakatoa air-sea waves: An example of pulse propagation in coupled systems. *Geophysical Journal of the Royal astronomical Society, 13*, 149–159.

Haskell, N. A. (1953). The dispersion of surface waves in multi-layered media. *Bulletin of the Seismological Society of America, 43*, 17–24.

Hébert, H., Reymond, D., Krien, Y., Vergoz, J., Schindelé, F., Roger, J., & Loevenbruck, A. (2009). The 15 August 2007 Peru earthquake and tsunami: Influence of the source characteristics on the tsunami heights. *Pure and Applied Geophysics, 166*, 211–232.

Holton, J. R. (2004). *Dynamic meteorology* (4th ed.). Elsevier Academic Press.

Kanamori, H., & Cipar, J. J. (1974). Focal process of the great Chilean earthquake, May 22, 1960. *Physics of the Earth and Planetary Interiors, 9*, 128–136.

Kanamori, H., Mori, J., & Harkrider, D. G. (1994). Excitation of atmospheric oscillations by volcanic eruptions. *Journal of Geophysical Research, 99*, 21947–21961.

Kittel, C., & Kroemer, H. (1980). *Thermal physics.* W.H. Freeman.

Kramp, C. (1808). *Eléments d'arithmétique universelle.* Thiriart.

Lamb, H. (1910). On atmospheric oscillations. *Proceedings of the Royal Society (London), Series A, 84*, 551–572.

Lamb, H. (1932). *Hydrodynamics* (6th ed.). Cambridge University Press.

Laplace, P. S. (1805). *Traîté de mécanique céleste* (Vol. 4). Duprat.

Lognonné, P., Clévédé, E., & Kanamori, H. (1998). Computation of seismograms and atmospheric oscillations by normal-mode summation for a spherical Earth model with realistic atmosphere. *Geophysical Journal International, 135*, 388–406.

Minzner, R. A., Champion, K. S. W., & Pond, H. L. (1959). *The ARDC model atmosphere.* Air Force Office of Scientific Research.

Nakamura, K., & Watanabe, H. (1961). Tsunami forerunner observed in case of the Chile Tsunami of 1960. In *Report on the Chilean Tsunami of May 24, 1960, as observed along the Coast of Japan.* Committee for Field Investigation of the Chilean Tsunami of 1960.

Newton, I. (1687). *Philosophiæ naturalis principa mathematica.* Strester.

Okal, E. A. (1982). Mode-wave equivalence and other asymptotic problems in tsunami theory. *Physics of the Earth and Planetary Interiors, 30*, 1–11.

Okal, E. A. (1988). Seismic parameters controlling far-field tsunami amplitudes: A review. *Natural Hazards, 1*, 67–96.

Okal, E. A. (2022). Air waves from the 2022 Tonga explosion: Theoretical studies and an oversight in the reporting of DART sensor data. *Seismological Research Letters, 93*, 1187–1188. [abstract].

Okal, E. A., & Talandier, J. (1991). Single-station estimates of the seismic moment of the 1960 Chilean and 1964 Alaskan earthquakes, using the mantle magnitude M_m. *Pure and Applied Geophysics, 136*, 103–126.

Pekeris, C. L. (1937). Atmospheric oscillations. *Proceedings of the Royal Society (London), Series A, 158*, 650–671.

Pekeris, C. L. (1939). The propagation of a pulse in the atmosphere. *Proceedings of the Royal Society (London), Series A, 171*, 434–449.

Press, F., & Harkrider, D. G. (1962). Propagation of acoustic-gravity waves in the atmosphere. *Journal of Geophysical Research, 67*, 3889–3908.

Rabinovich, A. B., Woodworth, P. L., & Titov, V. V. (2011). Deep-sea observations and modeling of the 2004 Sumatra tsunami in Drake Passage. *Geophysical Research Letters, 38*, L16604.

Saito, M. (1967). Excitation of free oscillations and surface waves by a point source in a vertically heterogeneous Earth. *Journal of Geophysical Research, 72*, 3689–3699.

Taylor, G. I. (1937). The oscillations of the atmosphere. *Proceedings of the Royal Society (London), Series A, 158*, 318–326.

Titov, V. V., Kânoğlu, U., & Synolakis, C. E. (2016). Development of MOST for real-time tsunami forecasting. *Journal of Waterways, Port and Coastal Engineering, 142*, 03116004.

Tsai, V. C., Ampuero, J.-P., Kanamori, H., & Stevenson, D. J. (2013). Estimating the effect of Earth elasticity and variable water density on tsunami speeds. *Geophysical Research Letters, 40*, 492–496.

UNESCO. (1981). Background papers and supporting data on the International Equation of State of seawater. *UNESCO Technical Papers in Marine Science, 38*, 192 pp., Paris.

Väisälä, V. (1925). Über die Wirkung der Windschwankungen auf die Pilotbeobachtungen. *Societas Scientiarium Fennica Commentationes, 2*, 1–46.

Ward, S. N. (1980). Relationships of tsunami generation and an earthquake source. *Journal of Physics of the Earth, 28*, 441–474.

Wares, G. W., Champion, K. W., Pond, H. L., & Cole, A. E. (1960). Model atmospheres. In *Handbook of geophysics* (pp. (1-1)–(1-43)). The Macmillan Co.

Watada, S. (2013). Tsunami speed variations in density-stratified compressible global oceans. *Geophysical Research Letters, 40*, 4001–4006.

Watada, S., Kusumoto, S., & Satake, K. (2014). Travel-time delay and initial phase reversal of distant tsunamis coupled with the self-gravitating elastic Earth. *Journal of Geophysical Research, Solid Earth, 119*, 4287–4310.

Watanabe, S., Hamilton, K., Sakazaki, T., & Nakano, M. (2022). First detection of the Pekeris internal global atmospheric resonance: Evidence for the 2022 Tonga eruption and from global reanalysis data. *Journal of Atmospheric Sciences, 79*, 3027–3043.

Wessel, P., & Smith, W. H. F. (1991). Free software helps map and display data. *Eos, Transactions of the American Geophysical Union, 72*, 441 and 445–446.

Wexler, H., & Hass, W. A. (1962). Global atmospheric pressure effects of the October 30, 1961, explosion. *Journal of Geophysical Research, 67*, 3875–3887.

Whipple, F. J. W. (1930). The great Siberian meteor and the waves, seismic and aerial, which it produced. *Quarterly Journal of the Royal Meteorological Society (London), 56*, 287–304.

Wiggins, R. A. (1976). A fast, new computational algorithm for free oscillations and surface waves. *Geophysical Journal of the Royal astronomical Society, 47*, 135–150.

Yamamoto, R. (1957). Microbarographic oscillation produced by the Soviet explosion of a hydrogen bomb on 22 November, 1955. *Bulletin of the American Meteorological Society, 38*, 536–539.